This paper appears as: Carlos Eduardo Rodríguez-Pardo and Gaurav Sharma. Color control functions for multiprimary displays I: Robustness analysis and optimization formulations. IEEE Trans. Image Proc., 29(1):1152--1163, 2020.DOI:10.1109/TIP.2019.2937067

Color Control Functions for Multiprimary Displays I: Robustness Analysis and Optimization Formulations

Carlos Eduardo Rodríguez-Pardo and Gaurav Sharma, *Fellow, IEEE*

***Abstract*—Color management for a multiprimary display requires, as a fundamental step, the determination of a color control function (CCF) that specifies control values for reproducing each color in the display's gamut. Multiprimary displays offer alternative choices of control values for reproducing a color in the interior of the gamut and accordingly alternative choices of CCFs. Under ideal conditions, alternative CCFs render colors identically. However, deviations in the spectral distributions of the primaries and the diversity of cone sensitivities among observers impact alternative CCFs differently, and, in particular, make some CCFs prone to artifacts in rendered images. We develop a framework for analyzing robustness of CCFs for multiprimary displays against primary and observer variations, incorporating a common model of human color perception. Using the framework, we propose analytical and numerical approaches for determining robust CCFs. First, via analytical development, we: (a) demonstrate that linearity of the CCF in tristimulus space endows it with resilience to variations, particularly, linearity can ensure invariance of the gray axis, (b) construct an axially linear CCF that is defined by the property of linearity over constant chromaticity loci, and (c) obtain an analytical form for the axially linear CCF that demonstrates it is continuous but suffers from the limitation that it does not have continuous derivatives. Second, to overcome the limitation of the axially linear CCF, we motivate and develop two variational objective functions for optimization of multiprimary CCFs, the first aims to preserve color transitions in the presence of primary/observer variations and the second combines this objective with desirable invariance along the gray axis, by incorporating the axially linear CCF. A companion Part II paper, presents an algorithmic approach for numerically computing optimal CCFs for the two alternative variational objective functions proposed here and presents results comparing alternative CCFs for several different $4, 5$, and 6 primary designs.**

***Index Terms*—robust color control function, control values, device variation, observer variation, multiprimary displays, display color management, variational optimization.**

I. Introduction

Compared with conventional displays that use a set of three red, green, and blue primaries for reproducing colors, multiprimary displays, i.e., display systems with four or more primaries, offer several advantages. Additional primaries can enlarge the gamut, i.e., the range of colors that the display can reproduce [2], [3]. Used in combination with multispectral capture, multiprimary displays can approximate the spectrum of a target object, reducing challenges due to variations in observer color perception [4]. Additionally, multiprimary displays have also been exploited to reduce power consumption [5], [6], to widen the effective viewing angle [7], and to increase spatial resolution [8], [9].

For three primary displays, each color can only be produced by a corresponding unique combination of the primaries and the display control values are, therefore, uniquely determined by the color to be reproduced. On the other hand, for a multiprimary display, several alternative combinations of primaries can reproduce a given color and, therefore, display control values are not uniquely determined by the color to be reproduced [10]. Spectral information about the reproduction target, if available, can guide the selection between alternative control values for the reproduction of a color. However, such information is rarely available in most color reproduction workflows, and other criteria are therefore used to select between multiple valid control values, to define a color control function (CCF) for the display that maps each color within the gamut to a corresponding unique control value that is used to reproduce the color. Other attributes of display performance, such as those mentioned in the preceding paragraph, can sometimes help to define the CCF. A number of alternative strategies have also been adopted for defining CCFs for multiprimary displays. The matrix switching methodology [11] offers an efficient algorithm for the computation of CCFs based on a pyramidal partition of the tristimulus gamut. An alternative strategy using a similar gamut decomposition in a linearized LAB space was presented in [12]. A methodology based on interpolations in equi-luminance planes to obtain smooth functions on color regions of linear transition was proposed in [13]. In [14] the center of gravity of a volume denoted as the metameric black is computed as the color control value, while [15] proposed a method based on a spherical average. For emissive multiprimary displays, CCFs that minimize optical power consumption were introduced in [16]–[18].

In this paper, we develop a mathematical framework for analyzing and optimizing the CCF for multiprimary displays, particularly taking into account robustness to primary (and observer) variations. It is important that the CCF design be robust to primary variations because variations in the spectral distribution of the primaries are inevitable in manufacturing processes, and additional changes in the primaries may be introduced over time as the display ages. Although, in an ideal setting, all CCFs are identical in their color reproduction behavior, in the presence of primary variations, poorly chosen CCFs can lead to artifacts in rendered images. In particular,

C.E. Rodríguez-Pardo is with the Department of Electrical and Computer Engineering, University of Rochester, Rochester, NY, 14627 USA (e-mail: c.rodriguezpardo@rochester.edu)

G. Sharma is with the Department of Electrical and Computer Engineering, Department of Computer Science, and Department of Biostatistics and Computational Biology, University of Rochester, Rochester, NY 14627, USA (e-mail: gaurav.sharma@rochester.edu)

A precursor to part of the work presented here appeared as [1].

smooth transitions in color are common in both natural and synthetic imagery and, for maintaining naturalness, it is critical that the smoothness in such color transitions be preserved in display renditions [19] despite the primary variations.

The work presented in this paper and its accompanying Part II companion paper [20] represents the first comprehensive framework for analyzing the robustness of CCFs for multiprimary displays. The developed framework not only leads to an entirely new variational approach for optimizing CCFs for multiprimary displays, but also provides key insights for CCFs previously proposed in the literature with alternative motivations, explaining both their strengths (e.g. the gray axis perceptual invariance for the matrix switching methodology [11]) and their shortcomings (e.g., the derivative discontinuities for the matrix switching methodology [11] and the lack of smoothness for the minimum power CCF [16]–[18]). Our analysis considers two aspects of robustness to primary variations: perceptual invariance along the gray axis and preservation of color transitions. In particular, we analytically demonstrate that linearity of the CCF in tristimulus space over the gray axis (a locus of constant chromaticity) ensures perceptual invariance of the gray axis in the presence of primary variations. Motivated by this observation, we construct the axially linear CCF, which is defined by the property of linearity over all constant chromaticity loci. Through analytical treatment we demonstrate that the axially linear CCF corresponds to a piece-wise linear transform, resulting in a pyramidal partitioning of the gamut, where the CCF is defined by a linear transformation, i.e., a matrix, over each partition, which coincides with the matrix switching methodology [11] developed previously from an alternative motivation. Furthermore, we show that while the axially linear CCF is continuous it suffers from localized derivative discontinuities that can create artifacts in renderings of smooth color transitions in the presence of primary variations. To overcome these limitations, we motivate and develop two variational objective functions for optimization of multiprimary CCFs; the first aims to preserve color transitions in the presence of primary/observer variations and the second combines this objective with desirable invariance along the gray axis by locally penalizing deviations from the axially linear CCF in the vicinity of the gray axis. Algorithms for numerical computation of the optimal CCFs and results are presented in a companion Part II paper [20].

This manuscript is organized as follows: Section II introduces the mathematical models for multiprimary displays in spectral and colorimetric representations, highlighting how primary and observer variations are modeled and formally defining CCFs. Salient aspects of perceptual representations of color that are relevant to the ensuing discussion are briefly summarized in Section III. The concepts introduced abstractly in Sections II and III are concretely illustrated via an example in Section IV, which also shows how the choice of the CCF can impact the effect of primary variations. In Section V, we establish that linearity of the CCF along the gray axis implies perceptual invariance of the gray axis to primary variations. Additionally, we demonstrate that if we extend the property of linearity from the single chromaticity corresponding to the gray axis to all loci of constant chromaticity, we obtain a specific CCF, the axially linear CCF, for which we derive an analytical expression and characterize its continuity and differentiability. In SectionVI we analyze the ability of CCFs to preserve perceptual color transitions in the presence of primary/observer variations and quantify this ability via a useful error metric that penalizes lack of smoothness in CCFs. Additionally, we propose a variational framework for obtaining optimal robust CCFs for multiprimary displays by minimizing the error metric or its variant that, with the objective of incorporating gray invariance, adds in a penalty for deviations from the axially linear CCF in the vicinity of the gray axis. The conclusions and summary of the main findings of this work are found in Section VII. Appendices A and B provide, respectively, relevant properties of the matrices that define the axially linear CCF and a derivation of the bound that forms the variational error metric characterizing the CCFs ability to preserve color transitions in the presence of primary variations. To assist readers, we summarize the symbols and acronyms used in this paper in Table I. Additionally, to better convey intuition and to improve accessibility of the mathematical development, we highlight key points and findings by italicizing these.

II. Display Modeling and Color Control Functions

For an additive display system with K ($K \geq 3$) primaries with spectral distributions $p_k(\lambda)$, where $1 \leq k \leq K$ and λ represents the wavelength, the spectra rendered by the display can be represented as a linear combination of the primaries as,

$$s(\boldsymbol{\alpha}, \lambda) = \sum_{k=1}^{K} \alpha_k p_k(\lambda)\,, \tag{1}$$

where α_k is the control value for the k^{th} primary, a value between 0 a 1 that indicates the relative intensity of the primary, and $\boldsymbol{\alpha} = [\alpha_1, \ldots, \alpha_K]^T$ is the vector of control values. A value of $\alpha_k = 1$ indicates that the k^{th} primary is at full intensity, while $\alpha_k = 0$, indicates that the k^{th} primary is turned off.

For the displayed spectrum $s(\boldsymbol{\alpha}, \lambda)$, the color perceived by an observer is commonly represented in the form of a "XYZ" tristimulus vector

$$\begin{aligned}\mathbf{t}(\boldsymbol{\alpha}) &\stackrel{\text{def}}{=} \begin{bmatrix} t_X(\boldsymbol{\alpha}) \\ t_Y(\boldsymbol{\alpha}) \\ t_Z(\boldsymbol{\alpha}) \end{bmatrix} \triangleq \begin{bmatrix} \int x(\lambda) s(\boldsymbol{\alpha}, \lambda)\, \mathrm{d}\lambda \\ \int y(\lambda) s(\boldsymbol{\alpha}, \lambda)\, \mathrm{d}\lambda \\ \int z(\lambda) s(\boldsymbol{\alpha}, \lambda)\, \mathrm{d}\lambda \end{bmatrix}, \\ &= \int \mathbf{x}(\lambda) s(\boldsymbol{\alpha}, \lambda)\, \mathrm{d}\lambda, \end{aligned} \tag{2}$$

where $\mathbf{x}(\lambda) = [x(\lambda), y(\lambda), z(\lambda)]^T$ is the vector of observer's (XYZ) color matching functions [21]. The notation $\mathbf{t}(\boldsymbol{\alpha})$ highlights the dependency of $\mathbf{t}$ on the choice of control values. The International Commission on Illumination (CIE) defines the color matching functions for a standard observer, denoted by $\bar{\mathbf{x}}(\lambda) = [\bar{x}(\lambda), \bar{y}(\lambda), \bar{z}(\lambda)]^T$, as typical averages of the population [22]. The corresponding vector of tristimulus values for the standard observer are referred to as the CIE XYZ tristimulus vector.

TABLE I: Symbols and Acronyms

Symbol/ Acronym	Description
K	Number of primaries
ζ	Generic real number
Color representation	
$\mathbf{t}=[t_X, t_Y, t_Z]$	3×1 color tristimulus vector
$\boldsymbol{\tau}=[\tau_L, \tau_{c_1}, \tau_{c_2}]$	3×1 color vector in opponent perceptual space
$\mathscr{C}=\{L, c_1, c_2\}$	Indices for perceptual color coordinates
$C_{\boldsymbol{\tau}}$	Chroma of $\boldsymbol{\tau}$, $C_{\boldsymbol{\tau}}=\sqrt{\tau_{c_1}^2+\tau_{c_2}^2}$
$\mathscr{F}_{\mathbf{w}}$	Tristimulus to perceptual space transform
x, y	CIE xy chromaticity coordinates
$\bar{\mathbf{P}}$	$3 \times K$ matrix of nominal primary tristimuli
$\Delta\mathbf{P}$	$3 \times K$ primary (tristimuli) variation matrix
$\mathbf{P}$	$3 \times K$ matrix of primaries $\mathbf{P}=\bar{\mathbf{P}}+\Delta\mathbf{P}$
$\hat{\mathbf{t}}/\hat{\boldsymbol{\tau}}$	3×1 display reproduced color in tristimulus/perceptual space
$\bar{\mathbf{w}}/\mathbf{w}$	3×1 tristimulus of nominal/display white
$\mathcal{G}/\mathcal{G}_{\mathscr{F}}$	Gamut in tristimulus/perceptual space
$\mathcal{Q}$, Q, $\mathbf{q}$	Quadrangle pyramid, pyramid parallelogram base, and origin of the base.
$\boldsymbol{\varphi}(\zeta)/\hat{\boldsymbol{\varphi}}(\zeta)$	Parametric representation of target/rendered color trajectory at ζ.
Control space	
CBS	Control Black Subspace
MCS	Metameric Control Set
CCF	Color Control Function
$\boldsymbol{\alpha}$	$K \times 1$ control vector
$\Omega(\mathbf{t})$	MCS for tristimulus $\mathbf{t}$
$\boldsymbol{\alpha}(\mathbf{t})/\boldsymbol{\alpha}^{\mathscr{F}}(\boldsymbol{\tau})$	CCF in tristimulus/perceptual space
$\boldsymbol{\beta}(\mathbf{t})/\boldsymbol{\beta}^{\mathscr{F}}(\boldsymbol{\tau})$	$(K-3) \times 1$ CBS representation of $\boldsymbol{\alpha}(\mathbf{t})/\boldsymbol{\alpha}^{\mathscr{F}}(\boldsymbol{\tau})$
Derivatives	
$\boldsymbol{\varphi}'(\zeta)/\hat{\boldsymbol{\varphi}}'(\zeta)$	Derivative of target trajectory/rendered curve at ζ.
$\nabla\alpha_k(\mathbf{t})/\nabla\alpha_k^{\mathscr{F}}(\boldsymbol{\tau})$	Gradient of the k^{th} component of the CCF in tristimulus/perceptual space at $\mathbf{t}/\boldsymbol{\tau}$.
$\mathbf{J}_{\boldsymbol{\alpha}}(\mathbf{t})/\mathbf{J}_{\boldsymbol{\alpha}^{\mathscr{F}}}(\boldsymbol{\tau})$	Jacobian of CCF in tristimulus/perceptual space at $\mathbf{t}/\boldsymbol{\tau}$.
$\mathbf{J}_{\mathscr{F}_{\mathbf{w}}(\hat{\mathbf{t}})}/\mathbf{J}_{\mathscr{F}_{\mathbf{w}}^{-1}(\boldsymbol{\tau})}$	Jacobian of (perceptual transformation)/(inverse perceptual transformation) at $\hat{\mathbf{t}}/\boldsymbol{\tau}$.

For the description of color representation and processing in this paper, we adopt and extend the vector systems notation prevalent in the signal processing community [23]–[25]. We denote by $\mathbf{p}_1, \ldots, \mathbf{p}_K$ the XYZ tristimulus vectors corresponding, respectively, to the primary's spectra $p_1(\lambda), \ldots, p_K(\lambda)$, where $\mathbf{p}_k = [p_{k,X}, p_{k,Y}, p_{k,Z}]^T$. Then the tristimulus vector $\mathbf{t}$ for the color reproduced by the display when driven by the control vector $\boldsymbol{\alpha}$ can be computed as [24]–[26]

$$\mathbf{t}(\boldsymbol{\alpha}) = \sum_{k=1}^{K} \alpha_k \mathbf{p}_k = \mathbf{P}\boldsymbol{\alpha}, \tag{3}$$

where $\mathbf{P}$ represents the $3 \times K$ primary matrix $\mathbf{P} = [\mathbf{p}_1, \mathbf{p}_2, \ldots, \mathbf{p}_K]$[1].

To render a desired color tristimulus $\mathbf{t}_0$ on the display, we need a control vector $\boldsymbol{\alpha}$ for such that $\mathbf{t}(\boldsymbol{\alpha}) = \mathbf{t}_0$, i.e., an inverse for the model in (3). The inverse is typically determined under the assumption of a CIE standard observer and for standardized nominal specification of the primaries. Deviations from these ideal values will typically result in errors in the rendered colors. To model such errors, we proceed as follows. The spectral distribution for the k^{th} primary is modeled as $p_k(\lambda) = \bar{p}_k(\lambda) + \Delta p_k(\lambda)$, where spectra function $\bar{p}_k(\lambda)$ corresponds to the nominal primary and $\Delta p_k(\lambda)$ to the spectral variation. Similarly the observer color matching functions are modeled as $\mathbf{x}(\lambda) = \bar{\mathbf{x}}(\lambda) + \Delta\mathbf{x}(\lambda)$, where $\Delta\mathbf{x}(\lambda)$ is the spectral deviation of the color matching functions from the CIE standard observer. From (1) and (2), we then obtain

$$\begin{aligned}\mathbf{t}(\boldsymbol{\alpha}) &= \left(\bar{\mathbf{P}} + \Delta\mathbf{P}\right)\boldsymbol{\alpha} \\ &= \mathbf{P}\boldsymbol{\alpha},\end{aligned} \tag{4}$$

where $\mathbf{P} = \bar{\mathbf{P}} + \Delta\mathbf{P}$, $\bar{\mathbf{P}} = [\bar{\mathbf{p}}_1, \bar{\mathbf{p}}_2, \ldots \bar{\mathbf{p}}_K]$ is the (nominal) primary matrix specification for the device, with

$$\bar{\mathbf{p}}_k = \int \bar{\mathbf{x}}(\lambda)\bar{p}_k(\lambda)\,\mathrm{d}\lambda, \tag{5}$$

and $\Delta\mathbf{P} = \Delta_{\mathcal{D}}\mathbf{P} + \Delta_{\mathcal{O}}\mathbf{P} + \Delta_{\mathcal{O},\mathcal{D}}\mathbf{P}$, with

$$\begin{aligned}\Delta_{\mathcal{D}}\mathbf{p}_k &= \int \bar{\mathbf{x}}(\lambda)\Delta p_k(\lambda)\,\mathrm{d}\lambda, \\ \Delta_{\mathcal{O}}\mathbf{p}_k &= \int \Delta\mathbf{x}(\lambda)\bar{p}_k(\lambda)\,\mathrm{d}\lambda, \\ \Delta_{\mathcal{O},\mathcal{D}}\mathbf{p}_k &= \int \Delta\mathbf{x}(\lambda)\Delta p_k(\lambda)\,\mathrm{d}\lambda.\end{aligned} \tag{6}$$

The *primary variation matrix* $\Delta\mathbf{P}$, which expresses the overall effect of the device and observer deviations, is the sum of three components: (a) $\Delta_{\mathcal{D}}\mathbf{P}$ attributable to the spectral deviations of the device primaries from their standard values, (b) $\Delta_{\mathcal{O}}\mathbf{P}$ attributable to the deviation of the observer's color matching functions from the CIE standard observer, and (c) $\Delta_{\mathcal{O},\mathcal{D}}\mathbf{P}$ attributable to the interaction between the spectral variation of the device primaries and the deviation of the observer.

Color control for the display makes use of the standardized primary matrix $\bar{\mathbf{P}}$. The unit hypercube $[0,1]^K$ defines the valid range of control values and the corresponding set of feasible XYZ tristimulus values defines the *display CIE XYZ (tristimulus) gamut*

$$\mathcal{G} \;=\; \left\{\mathbf{t} | \mathbf{t} = \bar{\mathbf{P}}\boldsymbol{\alpha}, \boldsymbol{\alpha} \in [0,1]^K\right\}, \tag{7}$$

i.e., the set of tristimuli that the (standardized) device can reproduce. The tristimulus gamut is a type of convex polytope [27] known as a zonotope [28], [29]. Specifically, for the $K = 3$ primary case, the tristimulus gamut is a parallelepiped. Reproducing a tristimulus $\mathbf{t}_0 \in \mathcal{G}$ requires the selection of a control vector $\boldsymbol{\alpha}_0$ to drive the display. In the three primary scenario, $\bar{\mathbf{P}}$ is a non-singular 3×3 matrix, and the desired control vector is uniquely determined as $\boldsymbol{\alpha}_0 = \bar{\mathbf{P}}^{-1}\mathbf{t}_0$. For a multiprimary display, various control vectors may be used to render a desired color $\mathbf{t}_0$. Specifically, we define the *metameric control set* (MCS) of $\mathbf{t}_0$, as the set

$$\Omega(\mathbf{t}_0) = \left\{\boldsymbol{\alpha} \in [0,1]^K \;\middle|\; \mathbf{t}_0 = \bar{\mathbf{P}}\boldsymbol{\alpha}\right\} \tag{8}$$

[1]We assume that any three columns from $\mathbf{P}$ are linearly independent.

of all feasible control vectors that reproduce the tristimulus $\mathbf{t}_0$ [18]. The MCS $\Omega(\mathbf{t}_0)$ is a convex polytope and can be alternatively represented as the convex hull of its vertices, viz.,

$$\Omega(\mathbf{t}_0) = \text{conv}(\boldsymbol{\nu}_1, \ldots, \boldsymbol{\nu}_{N_{\Omega(\mathbf{t}_0)}}) \stackrel{\text{def}}{=} \left\{ \sum_{i=1}^{N_{\Omega(\mathbf{t}_0)}} \kappa_i \boldsymbol{\nu}_1 \;\middle|\; 0 \le \kappa_i \le 1,\ \sum_{i=1}^{N_{\Omega(\mathbf{t}_0)}} \kappa_i = 1 \right\} \quad (9)$$

where $\text{conv}(\cdot)$ denotes the convex hull, and $\boldsymbol{\nu}_1, \ldots, \boldsymbol{\nu}_{N_{\Omega(\mathbf{t}_0)}} \in [0,1]^K$ are the vertices of the MCS polytope, with $N_{\Omega(\mathbf{t}_0)}$ denoting the number of vertices of $\Omega(\mathbf{t}_0)$.

Any control vector $\boldsymbol{\alpha}_0 \in \Omega(\mathbf{t}_0)$ can be chosen to render the desired color $\mathbf{t}_0$. A *color control function* (CCF) $\boldsymbol{\alpha}(\mathbf{t}) : \mathcal{G} \to [0,1]^K$ can be defined by selecting one control vector from $\Omega(\mathbf{t})$ for each tristimulus $\mathbf{t} \in \mathcal{G}$. Since $\Omega(\mathbf{t})$ may contain more than one element, multiple CCFs may be defined.

For comparing and contrasting alternative CCFs, we use the visualization methodology of [18], which allows CCFs for multiprimary displays to be visualized for common practical cases despite the fact that these are functions of dimensionality greater than three. The methodology relies on the observation that for any two CCFs $\boldsymbol{\alpha}_1(\cdot)$ and $\boldsymbol{\alpha}_2(\cdot)$, we have that $\bar{\mathbf{P}}\left(\boldsymbol{\alpha}_1(\mathbf{t}) - \boldsymbol{\alpha}_2(\mathbf{t})\right) = \mathbf{0}$, indicating that differences of control values are entirely contained within the null space of $\bar{\mathbf{P}}$, referred to as the *control black subspace (CBS)* [18]. Thus, differences between the functions lie entirely in the $(K-3)$ dimensional CBS and can be represented in terms of an orthonormal basis $\mathbf{B}$ for the CBS. Specifically, we can express the difference as $\boldsymbol{\alpha}_1(\mathbf{t}) - \boldsymbol{\alpha}_2(\mathbf{t}) = \mathbf{B}\mathbf{B}^T(\boldsymbol{\alpha}_1(\mathbf{t}) - \boldsymbol{\alpha}_2(\mathbf{t}))$. Therefore, the $(K-3)\times 1$ vector $\boldsymbol{\beta}(\mathbf{t}) = \mathbf{B}^T\left(\boldsymbol{\alpha}_1(\mathbf{t}) - \boldsymbol{\alpha}_2(\mathbf{t})\right)$ represents the difference in terms of the chosen basis coordinates $\mathbf{B}$, which can be visualized for $K = 4, 5, 6$ covering most practical cases of interest.

III. Perceptual Representation of Color

Color changes caused by primary variation are best assessed in a color space, where the distances and axes are perceptually meaningful. For our discussion, we represent the mapping from tristimulus values to a perceptual space by a nonlinear transformation $\mathscr{F}_{\mathbf{w}}(\cdot)$, where $\mathbf{w}$ denotes the *display white* tristimulus $\mathbf{w} = \sum_{k=1}^{K} \mathbf{p}_k$, obtained when all primaries are turned completely on. The dependence of the transformation on the white tristimulus allows modeling of the fact that human color vision adapts its response relative to the white. An effect of such adaptation is that a "white piece of paper is always perceived as white" over a rather broad range of changes in illumination. Some insight into the structure of the transformation $\mathscr{F}_{\mathbf{w}}(\cdot)$ is helpful for our subsequent discussion. Perceptual models of human vision are built in functional stages following the physiology of human vision [30], [31]. These models include three major stages: a model for chromatic adaptation to white in a tristimulus space, a channel wise nonlinearity in the chromatically adapted "tristimulus" space, and finally a transformation of the nonlinear transformed values as a three channel opponent encoding representation. The three channel opponent encoding $\boldsymbol{\tau} = [\tau_L, \tau_{c_1}, \tau_{c_2}]^T$ represents colors in terms of common perceptual correlates $\mathscr{C} = \{L, c_1, c_2\}$ of color appearance, viz., light-dark (τ_L), red-green (τ_{c_1}), and yellow-blue (τ_{c_2}). Figure 1 illustrates this model structure using the specific example of the CIELAB color space [22] for concrete illustration; although the structure is more universal than CIELAB. The perceptual representation of the color corresponding to a display control vector $\boldsymbol{\alpha}$ is given by

$$\boldsymbol{\tau}(\boldsymbol{\alpha}) = \mathscr{F}_{\mathbf{w}}\left(\mathbf{t}(\boldsymbol{\alpha})\right) = \boldsymbol{\Phi}\,\mathbf{f}\big(\mathbf{D}_{\mathbf{w}}^{-1}\mathbf{t}(\boldsymbol{\alpha})\big)\,, \quad (10)$$

where $\mathbf{D}_{\mathbf{a}}$ denotes a square diagonal matrix with the vector $\mathbf{a}$ as its diagonal, $\mathbf{f}(\mathbf{t}) = [f(t_X),\ f(t_Y),\ f(t_Z)]^T$ represents the channel-wise non-linear transformation, and the 3×3 matrix $\boldsymbol{\Phi}$ represents the opponent encoding.

In the space of adapted tristimulus values $\mathbf{D}_{\mathbf{w}}^{-1}\mathbf{t}$, the white tristimulus $\mathbf{w}$ becomes the vector $\mathbf{1} = [1,1,1]^T$ and the line segment $\zeta\mathbf{1}$ for $0 \le \zeta \le 1$ represents the *gray* or *achromatic* axis ranging from black ($\zeta = 0$) to white ($\zeta = 1$). In the tristimulus space, the gray axis can then be directly seen to correspond to the line segment $\zeta\mathbf{w}$, for $0 \le \zeta \le 1$. The opponent encoding is constrained such that τ_{c_1} and τ_{c_2} are 0 along this gray axis so in the perceptual space, the gray axis is represented by colors with a representation of the form $\boldsymbol{\tau} = [\tau_L, 0, 0]^T$. Additional correlates of perception can be defined from the opponent encoding, including chroma $C_{\boldsymbol{\tau}} = \sqrt{\tau_{c_1}^2 + \tau_{c_2}^2}$ (the radial distance to the gray axis) and hue $h_{\boldsymbol{\tau}} = \arctan(\tau_{c_2}/\tau_{c_1})$ (the angular position on a plane of constant lightness). We note that the commonly used CIELAB perceptual color space can be represented in this framework [22]. CIELUV, which is an alternative uniform color space standardized by the CIE [22], adopts a different structure with a subtractive white point normalization but has a gray axis identical to CIELAB due to which subsequent statements relating to the gray axis are applicable to both CIELAB and CIELUV. For CIELAB and CIELUV, the coordinate τ_L is referred to as *lightness* and ranges from 0 (black) to 100 (white) along the gray axis. In our scenarios of interest, the conclusions regarding the gray axis also hold, albeit approximately, for more recent color appearance models such as CIECAM02 [32] and CAM16 [33]. Observe that along the gray axis the proportions of the three tristimulus values are identical to those for the white point. The proportions of the three tristimulus values are conveniently represented as 2D *chromaticity* values [22], $[x, y]$, which are obtained for tristimulus value $\mathbf{t}$ as $x = t_X/(t_X + t_Y + t_Z)$ and $y = t_Y/(t_X + t_Y + t_Z)$. The gray axis then corresponds to points of a constant chromaticity. The gray axis has special perceptual significance as observers are particularly sensitive to perturbations in color variations along this axis.

In the perceptual color space, the set of colors the device can reproduce, is the *display (perceptual) gamut*

$$\mathcal{G}_{\mathscr{F}} \;=\; \left\{\boldsymbol{\tau} | \boldsymbol{\tau} = \mathscr{F}_{\bar{\mathbf{w}}}(\bar{\mathbf{P}}\boldsymbol{\alpha}), \boldsymbol{\alpha} \in [0,1]^K\right\}. \quad (11)$$

where $\bar{\mathbf{w}} = \sum_{k=1}^{K} \bar{\mathbf{p}}_k$, is the nominal display white.

Because $\mathscr{F}_{\mathbf{w}}(\cdot)$ is a one-to-one function, the CCF $\boldsymbol{\alpha}(\cdot)$ can equivalently be represented in perceptual space by a corresponding function $\boldsymbol{\alpha}^{\mathscr{F}}(\boldsymbol{\tau}) : \mathcal{G}_{\mathscr{F}} \to [0,1]^K$ defined for colors in the perceptual gamut as[2] $\boldsymbol{\alpha}^{\mathscr{F}}(\boldsymbol{\tau}) = \boldsymbol{\alpha}\left(\mathscr{F}_{\bar{\mathbf{w}}}^{-1}(\boldsymbol{\tau})\right)$,

[2]Since every CCF is defined in terms of the nominal primaries, to simplify notation, the nominal display white $\bar{\mathbf{w}}$ is implicit in $\boldsymbol{\alpha}^{\mathscr{F}}(\cdot)$.

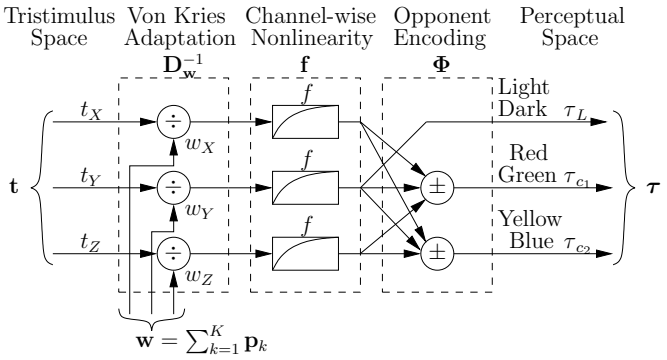

Fig. 1: Structure of common models for color perception. The model transforms a tristimulus $\mathbf{t} = [t_X, t_Y, t_Z]^T$ into a 3×1 vector $\boldsymbol{\tau} = [\tau_L, \tau_{c_1}, \tau_{c_2}]^T$, whose coordinates correspond to the three perceptual correlates of color appearance: light-dark (τ_L), red-green (τ_{c_1}), and yellow-blue (τ_{c_2}). Although the three stages in the model are common to most perceptual color spaces, the connectivity in the figure is based on CIELAB [22], where τ_L corresponds to CIE lightness which is obtained directly as a nonlinear transformation of the luminance t_Y (CIE Y value) because the CIE color matching function $\bar{y}(\lambda)$ was constructed to match the luminous efficiency function [22].

where $\mathscr{F}_{\mathbf{w}}^{-1}(\cdot)$ is the inverse of the perceptual transformation $\mathscr{F}_{\mathbf{w}}(\cdot)$. From (10) (and Fig. 1), we can see that

$$\mathscr{F}_{\mathbf{w}}^{-1}(\boldsymbol{\tau}) = \mathbf{D}_{\mathbf{w}}\, \mathbf{g}\big(\mathbf{\Phi}^{-1}\boldsymbol{\tau}\big)\,. \tag{12}$$

where $\mathbf{g}(\boldsymbol{\tau}) = [g(\tau_L),\ g(\tau_{c_1}),\ g(\tau_{c_2})]^T$, with $g(\cdot) = f^{-1}(\cdot)$.

IV. Example: CCF Dependence of Color Rendering in the Presence of Device Variation

We illustrate the concepts introduced in the preceding two sections by means of an example that also demonstrates how the choice of the CCF plays a significant role in determining the impact that primary variations have on rendered colors.

Consider the four primary display system of [34], which is defined by the primaries

$$\begin{aligned}\bar{\mathbf{P}} &= [\bar{\mathbf{p}}_1, \bar{\mathbf{p}}_2, \bar{\mathbf{p}}_3, \bar{\mathbf{p}}_4] \\ &\stackrel{\text{def}}{=} \begin{bmatrix} 0.5197 & 0.1661 & 0.0323 & 0.1447 \\ 0.2502 & 0.3995 & 0.2118 & 0.0465 \\ 0 & 0.0193 & 0.1268 & 0.8422 \end{bmatrix}. \end{aligned} \tag{13}$$

Consider a CCF $\boldsymbol{\alpha}_{\sim}^{\mathscr{F}}(\cdot)$ defined for each $\boldsymbol{\tau} \in \mathcal{G}_{\mathscr{F}}$ by randomly choosing a control vector from $\Omega(\mathscr{F}_{\bar{\mathbf{w}}}^{-1}(\boldsymbol{\tau}))$. For this four primary system ($K = 4$), the CBS is a one dimensional subspace with $\mathbf{B} = [-0.1462,\ 0.5202,\ -0.8337,\ 0.1136]^T$ as an orthonormal basis. As described in Section II, the CCF can be visualized in the 1D CBS with respect to (*wrt*) the basis $\mathbf{B}$. Figure 2(a) illustrates this by visualizing $\boldsymbol{\alpha}_{\sim}^{\mathscr{F}}(\boldsymbol{\tau})$ along the gray axis. The horizontal axis represents the location along the gray axis as the CIE lightness value τ_L (with the corresponding color given by $\boldsymbol{\tau} = [\tau_L, 0, 0]^T$), while the vertical axis corresponds to the value $\boldsymbol{\beta}_{\sim}^{\mathscr{F}}(\boldsymbol{\tau}) = \mathbf{B}^T\boldsymbol{\alpha}_{\sim}^{\mathscr{F}}(\boldsymbol{\tau})$, which represents the CBS component of the CCF *wrt* the basis $\mathbf{B}$.

When the primary variation matrix $\Delta\mathbf{P}$ is zero, all alternative CCFs (including $\boldsymbol{\alpha}_{\sim}^{\mathscr{F}}(\cdot)$) render the gray axis accurately as shown in Fig. 2(b). However, in the presence of primary variations this ideal behavior is compromised as illustrated in Fig. 2(c), which shows the rendering of the gray axis for the CCF $\boldsymbol{\alpha}_{\sim}^{\mathscr{F}}(\cdot)$ when the primary variation matrix $\Delta\mathbf{P}$ corresponds to a 5% random perturbation of each primary's magnitude. The rendered gray axis is no longer achromatic and suffers from objectionable variations in hue that are easily detected by the human visual system. Observe that the artifacts in the rendering coincide with the transitions of $\boldsymbol{\beta}_{\sim}^{\mathscr{F}}(\cdot)$. In the presence of the primary variation, the random transitions in $\boldsymbol{\beta}_{\sim}^{\mathscr{F}}(\cdot)$, that were hidden from the observer in the ideal no-perturbation scenario, are mapped into perceptible and quite objectionable variations.

To motivate the subsequent development in this paper, the plots and images in Figure 2 also illustrate the behavior for an alternative CCF $\boldsymbol{\alpha}_{\mathcal{A}}^{\mathscr{F}}(\cdot)$, whose construction will be detailed in Section V. For the gray axis, this alternative CCF is visualized in Fig. 2(a) as the dashed line representing $\boldsymbol{\beta}_{\mathcal{A}}^{\mathscr{F}}(\boldsymbol{\tau}) = \mathbf{B}^T\boldsymbol{\alpha}_{\mathcal{A}}^{\mathscr{F}}(\boldsymbol{\tau})$. For the CCF $\boldsymbol{\alpha}_{\mathcal{A}}^{\mathscr{F}}(\cdot)$, the rendering of the gray axis is perceptually invariant to primary variation and Fig. 2(b) therefore represents the gray axis rendered for this CCF both in the presence or absence of primary variation. Invariance to primary variation is a desirable condition for the selection of a CCF, and the motivation for the axially linear CCF $\boldsymbol{\alpha}_{\mathcal{A}}^{\mathscr{F}}(\cdot)$.

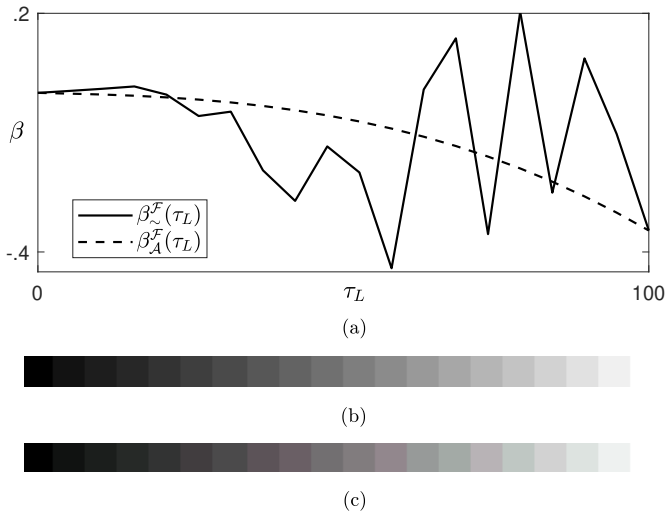

Fig. 2: Renderings of the gray axis by the four primary display defined in (13) using two different CCFs, $\boldsymbol{\alpha}_{\sim}^{\mathscr{F}}(\cdot)$ and $\boldsymbol{\alpha}_{\mathcal{A}}^{\mathscr{F}}(\cdot)$. (a) CBS visualization of both CCFs on the gray axis. (b) Rendering in ideal conditions using any CCF. (c) Rendering by $\boldsymbol{\alpha}_{\sim}^{\mathscr{F}}(\cdot)$ when considering primary variation equivalent to 5% the magnitude of the primaries. The rendering by $\boldsymbol{\alpha}_{\mathcal{A}}^{\mathscr{F}}(\cdot)$ with the same primary variations matches (a). The center of the color patches are spatially distributed to match the corresponding values of τ_L. The gray axis is represented by 20 patches uniformly spaced along the CIELAB/CIELUV lightness axis between $\tau_L = 0$ and $\tau_L = 100$. **To appreciate the color differences, please see the electronic version of the document**.

V. CCFs Robustness to Primary Variations: Gray Axis Invariance

Consider Fig. 3, which illustrates the reproduction of a target color $\boldsymbol{\tau}_0 \in \mathcal{G}_{\mathscr{F}}$ using a CCF $\boldsymbol{\alpha}(\cdot)$ (defined for the nominal primary matrix $\bar{\mathbf{P}}$). Using the nominal display white $\bar{\mathbf{w}} = \sum_{k=1}^{K} \bar{\mathbf{p}}_k$, the color specification $\boldsymbol{\tau}_0$ is mapped to a tristimulus $\mathbf{t}_0$, which in turn is mapped by the CCF into a corresponding control vector $\boldsymbol{\alpha}(\mathbf{t}_0)$ that drives the display. The reproduced color has a tristimulus $\hat{\mathbf{t}}_0 \stackrel{\text{def}}{=} \mathbf{t}\left(\boldsymbol{\alpha}\left(\mathbf{t}_0\right)\right) = \mathbf{P}\boldsymbol{\alpha}(\mathbf{t}_0)$, which potentially differs from $\mathbf{t}_0$ due to the variation $\Delta\mathbf{P}$ in the actual display primaries compared with the nominal primaries. A perceptual representation $\hat{\boldsymbol{\tau}}_0$ of the rendered tristimulus $\hat{\mathbf{t}}_0$ is obtained via the transformation $\mathscr{F}_{\mathbf{w}}(\cdot)$, specified by the display white $\mathbf{w} = \sum_{k=1}^{K} \mathbf{p}_k$, which is also potentially impacted by the display primary variation.

A. Linear CCFs and Gray Axis Perceptual Invariance

Consider a CCF $\boldsymbol{\alpha}(\mathbf{t})$ that is linear[3] along the line segment joining two in-gamut tristimuli $\mathbf{t}_a$ and $\mathbf{t}_b$. That is, for every $0 \leq \zeta \leq 1$, $\mathbf{t}_0 = (1-\zeta)\mathbf{t}_a + \zeta\mathbf{t}_b$

$$\boldsymbol{\alpha}\left(\mathbf{t}_0\right) = (1-\zeta)\boldsymbol{\alpha}(\mathbf{t}_a) + \zeta\boldsymbol{\alpha}(\mathbf{t}_b). \tag{14}$$

Pre-multiplying (14) by $\mathbf{P}$, we can see that the tristimulus $\hat{\mathbf{t}}_0 = \mathbf{t}\left(\boldsymbol{\alpha}\left(\mathbf{t}_0\right)\right)$ produced by the display in response to the control vector $\boldsymbol{\alpha}\left(\mathbf{t}_0\right)$ is given by

$$\hat{\mathbf{t}}_0 = (1-\zeta)\hat{\mathbf{t}}_a + \zeta\hat{\mathbf{t}}_b, \tag{15}$$

where $\hat{\mathbf{t}}_a = \mathbf{t}\left(\boldsymbol{\alpha}(\mathbf{t}_a)\right)$ and $\hat{\mathbf{t}}_b = \mathbf{t}\left(\boldsymbol{\alpha}(\mathbf{t}_b)\right)$ are the tristimuli produced by the display in response to the control vectors $\boldsymbol{\alpha}\left(\mathbf{t}_a\right)$ and $\boldsymbol{\alpha}\left(\mathbf{t}_b\right)$, respectively. Note that (15) indicates that $\hat{\mathbf{t}}_0$ lies upon and splits the line segment joining $\hat{\mathbf{t}}_a$ and $\hat{\mathbf{t}}_b$ in the same proportion that $\mathbf{t}_0$ splits the line segment joining $\mathbf{t}_a$ and $\mathbf{t}_b$. Thus, over line segments for which the CCF is linear, tristimuli maintain the same proportionality irrespective of perturbations in the primaries. This *proportionality preservation property* is particularly relevant and advantageous when the line segment under consideration matches the gray axis, i.e., $\mathbf{t}_a = \mathbf{0}$ and $\mathbf{t}_b = \bar{\mathbf{w}}$. For a CCF that is linear along the gray axis, points on the line segment and their corresponding reproductions are given by $\mathbf{t}_0 = \zeta\bar{\mathbf{w}}$ and $\hat{\mathbf{t}}_0 = \zeta\mathbf{w}$, respectively, for $0 \leq \zeta \leq 1$. The Von Kries chromatic adaptation described in Section III maps both $\mathbf{t}_0$ and $\hat{\mathbf{t}}_0$ to the same adapted tristimulus $\zeta\mathbf{1}$, and consequently, the corresponding perceptual representations match each other ($\hat{\boldsymbol{\tau}}_0 = \boldsymbol{\tau}_0$) regardless of the primary variation. Therefore, *linearity of the CCF along the gray axis implies perceptual invariance of the gray axis to primary variations*.

As described in Section III, the gray axis in fact corresponds to a constant chromaticity locus. Motivated by this observation, *we construct a specific CCF, the axially linear CCF $\boldsymbol{\alpha}_{\mathcal{A}}(\cdot)$, that is completely defined by the characteristic that it is linear over the loci of constant chromaticity.*

[3]Technically, we should characterize the CCF as "affine" but in the interest of maintaining consistency with the subsequent discussion, we resort to a minor abuse of terminology.

B. The Axially Linear CCF $\boldsymbol{\alpha}_{\mathcal{A}}(\cdot)$

We start by recalling that the control vector is uniquely defined for any color on the gamut surface [35], and thus $\boldsymbol{\alpha}_{\mathcal{A}}(\cdot)$ is uniquely defined on the gamut surface. Furthermore, observe that given any two in-gamut tristimuli $\mathbf{t}_a$ and $\mathbf{t}_b$ and corresponding control vectors $\boldsymbol{\alpha}(\mathbf{t}_a)$ and $\boldsymbol{\alpha}(\mathbf{t}_b)$, Equation (14) produces (feasible) control vectors for tristimuli along the line segment joining $\mathbf{t}_a$ and $\mathbf{t}_b$. It therefore follows that any CCF is linear over line segments lying completely on the gamut surface. Next we obtain the CCF $\boldsymbol{\alpha}_{\mathcal{A}}(\cdot)$ for tristimuli located in the interior of the gamut. The process can be understood by referring to Fig. 4. For a tristimulus $\mathbf{t}$ in the interior of the gamut, all nonzero points of matching chromaticity are given by $\gamma\mathbf{t}$, with $\gamma > 0$. Given that the gamut is convex and includes $\mathbf{0}$, only one of these tristimuli $\mathbf{t}_{\mathcal{E}} \stackrel{\text{def}}{=} \gamma_{\mathcal{E}}\mathbf{t}$ lies on the gamut surface. Now, $\boldsymbol{\alpha}_{\mathcal{A}}(\mathbf{t}_{\mathcal{E}})$ is defined by the uniqueness of control vectors for the gamut surface. From linearity of the CCF $\boldsymbol{\alpha}_{\mathcal{A}}(\cdot)$ along the line segment between $\mathbf{0}$ and $\mathbf{t}_{\mathcal{E}}$ (which is a locus of constant chromaticity), it follows that $\boldsymbol{\alpha}_{\mathcal{A}}(\mathbf{t}) = \boldsymbol{\alpha}_{\mathcal{A}}\left((1/\gamma_{\mathcal{E}})\mathbf{t}_{\mathcal{E}}\right) = (1/\gamma_{\mathcal{E}})\boldsymbol{\alpha}_{\mathcal{A}}(\mathbf{t}_{\mathcal{E}}) = \left(\|\mathbf{t}\| / \|\mathbf{t}_{\mathcal{E}}\|\right)\boldsymbol{\alpha}_{\mathcal{A}}(\mathbf{t}_{\mathcal{E}})$.

When the CCF $\boldsymbol{\alpha}_{\mathcal{A}}(\cdot)$ is used for a display with potential variation in the primaries, the proportionality preservation property applies. Specifically, to reproduce a desired tristimulus $\mathbf{t} = (1/\gamma_{\mathcal{E}})\mathbf{t}_{\mathcal{E}}$ the control vector $\boldsymbol{\alpha}_{\mathcal{A}}(\mathbf{t}) = (1/\gamma_{\mathcal{E}})\boldsymbol{\alpha}_{\mathcal{A}}(\mathbf{t}_{\mathcal{E}})$ is invoked and the tristimulus actually produced by the display is given by $\hat{\mathbf{t}} = \mathbf{P}\boldsymbol{\alpha}_{\mathcal{A}}\left(\mathbf{t}\right) = (1/\gamma_{\mathcal{E}})\hat{\mathbf{t}}_{\mathcal{E}}$, where $\hat{\mathbf{t}}_{\mathcal{E}} = \mathbf{P}\boldsymbol{\alpha}_{\mathcal{A}}\left(\mathbf{t}_{\mathcal{E}}\right)$. This is illustrated in Fig. 4: requested tristimuli on the line segment between $\mathbf{0}$ and $\mathbf{t}_{\mathcal{E}}$ are rendered proportionally on the line segment between $\mathbf{0}$ and $\hat{\mathbf{t}}_{\mathcal{E}}$. The observation and the figure also highlight another important conclusion; *regardless of any primary variation, the CCF $\boldsymbol{\alpha}_{\mathcal{A}}\left(\cdot\right)$ maps in-gamut tristimuli of constant chromaticity into control vectors that drive the display to produce tristimulus with constant chromaticity.*

C. $\mathcal{A}$-Pyramid Partitioning and Matrix Switching for the CCF $\boldsymbol{\alpha}_{\mathcal{A}}(\cdot)$

In the preceding subsection, we constructed the axially linear CCF $\boldsymbol{\alpha}_{\mathcal{A}}(\cdot)$ based on the defining characteristic of linearity along loci of constant chromaticity. Next, we establish that *the CCF $\boldsymbol{\alpha}_{\mathcal{A}}(\cdot)$ can alternatively be represented by partitioning the gamut into a specific set of quadrangle pyramids, which we refer to as the $\mathcal{A}$ pyramids, where over each pyramid the CCF $\boldsymbol{\alpha}_{\mathcal{A}}(\cdot)$ is a linear transform specified by a $K \times 3$ matrix.*

For points on the gamut surface, control vectors are uniquely defined. Thus, for any tristimulus $\mathbf{t}$ on the gamut surface, $\boldsymbol{\alpha}_{\mathcal{A}}(\mathbf{t})$ is defined by the unique control vector for $\mathbf{t}$. Let $\mathbf{t}$ be a point in the interior of the gamut, and let $\mathbf{t}_{\mathcal{E}} = \gamma_{\mathcal{E}}\mathbf{t}$ be the point of matching chromaticity on the gamut surface, as described in Section V-B. As seen in Fig. 5, $\mathbf{t}_{\mathcal{E}}$ lies on a parallelogram $Q = \{\mathbf{q} + \zeta\mathbf{p}_i + \mu\mathbf{p}_j \,|\, 0 \leq \zeta, \mu \leq 1\}$ that forms a facet of the gamut, where the primaries $\mathbf{p}_i$ and $\mathbf{p}_j$ ($1 \leq i < j \leq K$) span the parallelogram located at "origin" $\mathbf{q}$ (see the parallelogram in Fig. 5 bounded by blue lines). We can write $\mathbf{q} = \sum_{k=1}^{K} \chi_k\mathbf{p}_k = \mathbf{P}\boldsymbol{\chi}$, where $\boldsymbol{\chi} = [\chi_1, \ldots, \chi_K]^T$ is a binary-valued vector with $\chi_k = 0/1$ indicating whether the primary $\mathbf{p}_k$ contributes to the origin of the facet or not, respectively. We note that $\chi_i = \chi_j = 0$; $\boldsymbol{\chi} \neq \mathbf{0}$; and the

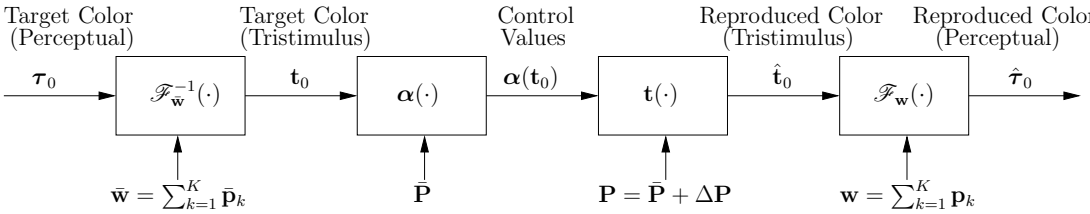

Fig. 3: Steps in the reproduction of a in-gamut color using a CCF $\boldsymbol{\alpha}(\cdot)$. A specified color $\boldsymbol{\tau}_0 \in \mathcal{G}_{\mathscr{F}}$ is mapped to a corresponding tristimulus value $\mathbf{t}_0$ using the nominal display white $\bar{\mathbf{w}}$. The display is driven with the control values $\boldsymbol{\alpha}(\mathbf{t}_0)$. The reproduced color has a tristimulus $\hat{\mathbf{t}}_0$, which is then mapped to a corresponding perceptual value $\hat{\boldsymbol{\tau}}_0$ using the display white $\mathbf{w}$.

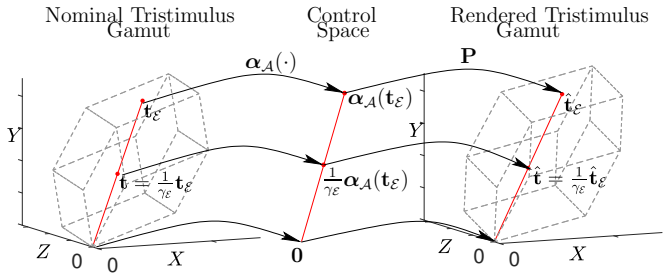

Fig. 4: Construction and properties of the CCF $\boldsymbol{\alpha}_{\mathcal{A}}(\cdot)$ that is linear along line segments constituting constant chromaticity loci. The region inside the wire-frame on the left represents the nominal display gamut in CIE XYZ tristimulus space for the $K = 4$ primary display used in the example of Section IV. For a tristimulus $\mathbf{t}$ in the interior of this gamut, the red line segment from $\mathbf{0}$ to $\mathbf{t}_{\mathcal{E}}$ represents the points $\{\gamma\mathbf{t} \in \mathcal{G} \mid \gamma > 0\}$ of matching chromaticity, where $\mathbf{t}_{\mathcal{E}} = \gamma_{\mathcal{E}}\mathbf{t}$ lies on the gamut surface. The uniqueness of control values on the gamut surface defines $\boldsymbol{\alpha}_{\mathcal{A}}(\mathbf{t}_{\mathcal{E}})$ and $\boldsymbol{\alpha}_{\mathcal{A}}(\mathbf{0}) = \mathbf{0}$. Linearity of $\boldsymbol{\alpha}_{\mathcal{A}}(\cdot)$ defines the control values for $\mathbf{t}$ as $\boldsymbol{\alpha}_{\mathcal{A}}(\mathbf{t}) = (1/\gamma_{\mathcal{E}})\boldsymbol{\alpha}_{\mathcal{A}}(\mathbf{t}_{\mathcal{E}})$. Consequently, as depicted in the figure, the CCF $\boldsymbol{\alpha}_{\mathcal{A}}(\cdot)$ maps, in a proportionality preserving fashion, the constant chromaticity red line segment on the left onto a corresponding line in the control space from $\mathbf{0}$ to $\boldsymbol{\alpha}_{\mathcal{A}}(\mathbf{t}_{\mathcal{E}})$, depicted as the red line in the center of the figure. When the display, with potential variation in the primaries, is driven by the control vector $\boldsymbol{\alpha}_{\mathcal{A}}(\mathbf{t})$ intended to reproduce the tristimulus $\mathbf{t}$, the tristimulus actually produced is $\hat{\mathbf{t}} = \mathbf{P}\boldsymbol{\alpha}_{\mathcal{A}}(\mathbf{t}) = (1/\gamma_{\mathcal{E}})\hat{\mathbf{t}}_{\mathcal{E}}$, where $\hat{\mathbf{t}}_{\mathcal{E}} = \mathbf{P}\boldsymbol{\alpha}_{\mathcal{A}}(\mathbf{t}_{\mathcal{E}})$. The region inside of the wire-frame on the right represents the rendered tristimulus gamut $\mathcal{G}$ and the red line within this gamut represents a constant chromaticity locus to which the CCF $\boldsymbol{\alpha}_{\mathcal{A}}(\cdot)$ renders the constant chromaticity line segment on the left in a proportionality preserving fashion.

vectors $\mathbf{q}$, $\mathbf{p}_i$, and $\mathbf{p}_j$ are linearly independent. Because $\mathbf{t}_{\mathcal{E}} \in Q$, there exist ζ and μ, $0 \le \zeta, \mu \le 1$, such that

$$\mathbf{t}_{\mathcal{E}} = \mathbf{q} + \zeta\mathbf{p}_i + \mu\mathbf{p}_j = \mathbf{P}\left(\boldsymbol{\chi} + \zeta\mathbf{e}_i + \mu\mathbf{e}_j\right), \tag{16}$$

where $\mathbf{e}_k$ denotes the $K \times 1$ binary vector whose k^{th} entry is 1 and all other entries are 0. From (16) and the uniqueness of control vectors on gamut the surface, it follows that

$$\boldsymbol{\alpha}_{\mathcal{A}}\left(\mathbf{t}_{\mathcal{E}}\right) = \boldsymbol{\chi} + \zeta\mathbf{e}_i + \mu\mathbf{e}_j. \tag{17}$$

Now, linearity of $\boldsymbol{\alpha}_{\mathcal{A}}(\cdot)$ along the locus of constant chromaticity of $\mathbf{t}$ implies that

$$\boldsymbol{\alpha}_{\mathcal{A}}(\mathbf{t}) = \frac{1}{\gamma_{\mathcal{E}}}\boldsymbol{\alpha}_{\mathcal{A}}\left(\mathbf{t}_{\mathcal{E}}\right) = \frac{1}{\gamma_{\mathcal{E}}}\left(\boldsymbol{\chi} + \zeta\mathbf{e}_i + \mu\mathbf{e}_j\right) = \frac{1}{\gamma_{\mathcal{E}}}\mathbf{A}\mathbf{v}, \tag{18}$$

where $\mathbf{A} = [\boldsymbol{\chi},\ \mathbf{e}_i,\ \mathbf{e}_j]$ is a $K \times 3$ matrix, and $\mathbf{v} = [1,\ \zeta,\ \mu]^T$. From (16) $\mathbf{t}$ can also be alternatively written as

$$\mathbf{t} = \frac{1}{\gamma_{\mathcal{E}}}\mathbf{t}_{\mathcal{E}} = \frac{1}{\gamma_{\mathcal{E}}}\left(\mathbf{q} + \zeta\mathbf{p}_i + \mu\mathbf{p}_j\right) = \frac{1}{\gamma_{\mathcal{E}}}\mathbf{M}\mathbf{v}, \tag{19}$$

where $\mathbf{M} = [\mathbf{q},\ \mathbf{p}_i,\ \mathbf{p}_j] = \mathbf{P}\mathbf{A}$ is a 3×3 nonsingular matrix. Thus $\mathbf{v} = \gamma_{\mathcal{E}}\mathbf{M}^{-1}\mathbf{t}$, and using this expression in (18), we obtain

$$\boldsymbol{\alpha}_{\mathcal{A}}(\mathbf{t}) = \mathbf{A}\mathbf{M}^{-1}\mathbf{t}. \tag{20}$$

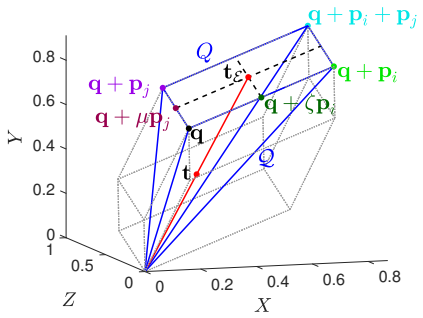

Fig. 5: The $\mathcal{A}$ quadrangle pyramid $\mathcal{Q}$ corresponding to a tristimulus $\mathbf{t}$ and determination of the matrix specifying the CCF $\boldsymbol{\alpha}_{\mathcal{A}}(\cdot)$ over $\mathcal{Q}$. The region inside the solid demarcated by the dashed gray lines shows the gamut for the four primary system introduced Section IV. For a tristimulus $\mathbf{t}$ the locus of matching chromaticity is indicated by the red line in the figure, which intersects with the gamut surface at a point $\mathbf{t}_{\mathcal{E}}$ lying on the facet Q of the gamut corresponding to the parallelogram bounded by the blue lines. Over the quadrangle pyramid $\mathcal{Q}$ formed with the parallelogram Q as the base and $\mathbf{0}$ as the apex (also demarcated by blue lines), the CCF $\boldsymbol{\alpha}_{\mathcal{A}}(\cdot)$ can be specified by a $K \times 3$ matrix (see text for details).

Observe that the matrices $\mathbf{A}$ and $\mathbf{M}$ used in the right-hand-side of (20) are determined by the parallelogram surface facet Q. Thus we see that over the quadrangle pyramid $\mathcal{Q}$ formed by using the parallelogram Q as the base and $\mathbf{0}$ as the apex (demarcated by the blue lines in Fig.5), the CCF $\boldsymbol{\alpha}_{\mathcal{A}}(\cdot)$ corresponds to the linear transform specified by the $K \times 3$ matrix $\mathbf{A}\mathbf{M}^{-1}$. Accordingly, we refer to $\mathcal{Q}$ as an $\mathcal{A}$ quadrangle pyramid of the gamut $\mathcal{G}$ and $\mathbf{A}\mathbf{M}^{-1}$ as the matrix that *specifies*

the CCF $\boldsymbol{\alpha}_{\mathcal{A}}(\cdot)$ over the $\mathcal{A}$-pyramid $\mathcal{Q}$. The complete gamut $\mathcal{G}$ (shown by the dashed lines in Fig.5), can be partitioned into $\mathcal{A}$ quadrangle pyramids, one pyramid for each (parallelogram-shaped) gamut surface facet that does not include the origin, and the CCF $\boldsymbol{\alpha}_{\mathcal{A}}(\cdot)$ can be specified as a set of $K\times 3$ matrices, one for each pyramid. Figure 6 illustrates this partitioning for a $K = 4$ primary gamut. For the $K = 3$ primary case, the CCF can also be formulated in the framework adopted in this section; for this case, the matrices are identical for each of the pyramids. However, for $K \geq 4$ there are multiple matrices and at most two of the pyramidal regions can have the same matrix for the CCF specification. Both results are established in Appendix A.

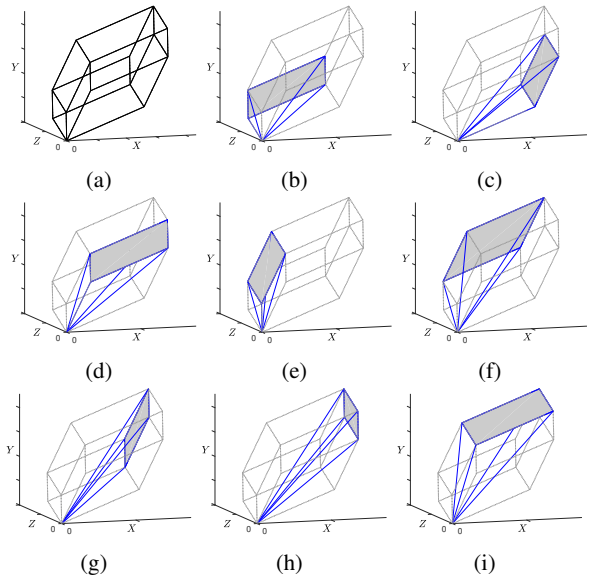

Fig. 6: The decomposition of the gamut of the four primary display system introduced in Section IV into $\mathcal{A}$ quadrangle pyramids. (a) The gamut of the four primary system, represented as the (region inside) the black wireframe. (b)–(i) The eight $\mathcal{A}$ quadrangle pyramids forming a partitioning of the gamut, illustrated as individual plots. Each $\mathcal{A}$ quadrangle pyramid is demarcated by (the region inside) blue lines. The base parallelogram of each pyramid, which forms a surface facet for the gamut, is shown by gray shading (which occludes points/lines behind the base from the reader's perspective). Each pyramid is shown in the context of the overall gamut which is demarcated by dashed gray lines. The gamut has twelve facets: four have their origin $\mathbf{q}$ at $\mathbf{0}$ and these cannot correspond to any pyramids with $\mathbf{0}$ as its base, four have their origins $\mathbf{q}$ as one of the primaries and these correspond to the quadrangle pyramids (b)–(e), and four have their origins $\mathbf{q}$ as the sums two primaries and these correspond to the quadrangle pyramids (f)–(i) that intersect with the white point.

We note that following a different motivation and approach, the *Matrix Switching* (MS) methodology [11] obtained a partitioning of the gamut identical to the one developed for the CCF $\boldsymbol{\alpha}_{\mathcal{A}}(\cdot)$ in the preceding discussion and also, an equivalent CCF specified as a set of matrices, one for each quadrangle pyramid. Specifically, the MS approach [11] was motivated by the need for a computationally efficient methodology for resolving the degeneracy of control values for multiprimary displays, which was accomplished by also developing a 2D look-up-table in chromaticity space that identifies the quadrangle pyramid, and thereby the matrix to be used, for a given tristimulus vector.

While the matrix switching between pyramidal regions maintains continuity of the CCF $\boldsymbol{\alpha}_{\mathcal{A}}(\cdot)$, as shown in Appendix A, it does not maintain continuity of the first derivative, which can lead to artifacts in display renderings under primary variation. Figure 7 illustrates this using the example of Section IV for a CIELUV v^* ramp that comprises (uniformly spaced points on) a line segment in the CIELUV perceptual gamut $\mathcal{G}_{\mathscr{F}}$ parallel to the CIELUV v^* (τ_{c_2}) axis and having constant CIELUV lightness $\tau_L = 75$, and CIELUV $u^* = \tau_{c_1} = 0$. The CCF $\boldsymbol{\alpha}_{\mathcal{A}}^{\mathscr{F}}(\boldsymbol{\tau}) \stackrel{\text{def}}{=} \boldsymbol{\alpha}_{\mathcal{A}}(\mathscr{F}_{\mathbf{w}}^{-1}(\boldsymbol{\tau}))$ exhibits a piece-wise linear behavior along this color trajectory, as shown by the CBS visualization in Fig. 7(a). Changes in the slope coincide with transitions between different pyramidal regions. Fig. 7(b) illustrates the rendering of the line segment for the nominal primaries ($\bar{\mathbf{P}}$) (under any CCF), and Fig. 7(c) illustrates the rendering for primaries that vary from the nominal by 10% in magnitude. Note that former ramp consists of smooth transitions between opposite hue colors, while this smoothness is compromised in the latter ramp, particularly over the region $0 \leq \tau_{c_2} \leq 50$, where the rendered ramp exhibits colors whose hue is clearly distinct from the hue of the extremes of the ramp.

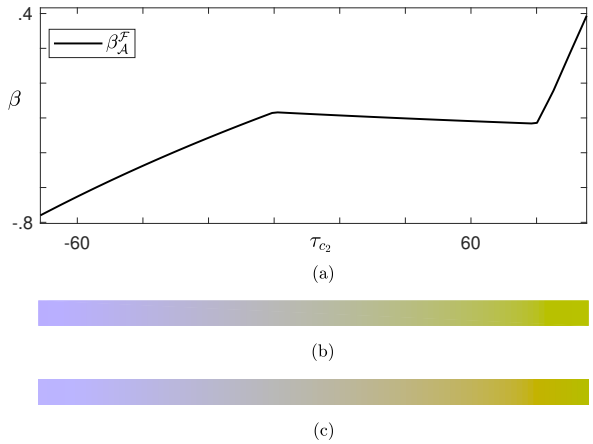

Fig. 7: Discontinuity of the first derivatives of $\boldsymbol{\alpha}_{\mathcal{A}}(\cdot)$ leads to artifacts in renderings under primary variation. (a) CBS visualization for $\boldsymbol{\alpha}_{\mathcal{A}}(\cdot)$ on a line segment with constant CIELUV lightness $L^* = 75$ (τ_L), along the CIELUV v^* (τ_{c_2}) axis. The tristimulus for this trajectory form a line segment that crosses different pyramids. Note that $\boldsymbol{\alpha}_{\mathcal{A}}^{\mathscr{F}}(\boldsymbol{\tau})$ is a piece-wise linear function, and the changes in slope corresponds to transition of pyramids (matrix switching). (b) Rendering of the trajectory when $\boldsymbol{\alpha}_{\mathcal{A}}^{\mathscr{F}}(\cdot)$ drives the nominal display. (c) Corresponding rendering when the primaries vary 10% in magnitude from nominal. Note the artifacts over the region $0 \leq \tau_{c_2} \leq 50$, where the rendered ramp exhibits colors whose hue is clearly distinct from the hue of the extremes of the ramp. **To appreciate the color differences, please see the electronic version of the document**.

As smooth transitions in color are common in both natural and synthetic imagery, it is important that the smoothness in such color transitions be preserved in the corresponding display renditions. Motivated by this observation, in the next section we establish desirable characteristics for a CCF that preserve the smoothness of color trajectories in display renditions under primary variation, and present strategies for its computation.

VI. Optimization Formulations for Robust CCFs

Consider a path in perceptual color space described parametrically by a function $\boldsymbol{\varphi}(\zeta) : \mathcal{D} \to \mathcal{G}_{\mathscr{F}}$, where $\mathcal{D}$ represents an interval of the real line $\mathbb{R}$. As ζ traverses the interval $\mathcal{D}$ monotonically, the trajectory of $\boldsymbol{\varphi}(\zeta)$ traces the desired path in color space. We assume that $\boldsymbol{\varphi}(\cdot)$ is continuous and differentiable. When the CCF $\boldsymbol{\alpha}^{\mathscr{F}}(\cdot)$ is used on the multiprimary display, the *target trajectory* $\boldsymbol{\varphi}(\cdot)$ is displayed as the *rendered curve* given by (see Fig 3)

$$\hat{\boldsymbol{\varphi}}(\zeta) = \mathscr{F}_{\mathbf{w}}\left(\mathbf{P}\boldsymbol{\alpha}^{\mathscr{F}}(\boldsymbol{\varphi}(\zeta))\right). \tag{21}$$

It is desirable that the transitions in the target and the rendered curves should match, even though absolute accuracy of the rendered color may be partly compromised by the primary variations. Because the transitions can be characterized locally by derivatives, the *deviation vector*

$$\boldsymbol{\delta}(\zeta) \stackrel{\text{def}}{=} \hat{\boldsymbol{\varphi}}'(\zeta) - \boldsymbol{\varphi}'(\zeta), \tag{22}$$

represents the difference between the color transitions for the target and rendered curves at parameter value ζ. To have a rendered curve whose transitions closely match that of the target curve, it is desirable to minimize the norm of the deviation $\boldsymbol{\delta}(\cdot)$. Note that if $\boldsymbol{\varphi}(\zeta)$ represents a trajectory along the gray axis and $\boldsymbol{\alpha}^{\mathscr{F}}(\cdot)$ is the axially linear CCF, $\boldsymbol{\alpha}^{\mathscr{F}}(\cdot) = \boldsymbol{\alpha}^{\mathscr{F}}_{\mathcal{A}}(\cdot)$, then, as discussed in Section V-B, we have $\hat{\boldsymbol{\varphi}}'(\zeta) = \boldsymbol{\varphi}'(\zeta)$ and it follows that $\boldsymbol{\delta}(\zeta) = \mathbf{0}$.

In general, the CCF cannot be constructed so as to ensure $\boldsymbol{\delta}(\zeta) = \mathbf{0}$ over the entire gamut. However, we can obtain a meaningful bound that then motivates an objective function for optimizing the CCF. Specifically, as shown in Appendix B, we can decompose the deviation vector as $\boldsymbol{\delta}(\zeta) = \boldsymbol{\delta}_0(\zeta) + \boldsymbol{\delta}_{\boldsymbol{\alpha}}(\zeta)$, where the term $\boldsymbol{\delta}_0(\zeta)$ depends only indirectly on the CCF through the changes in adaptation, and the term $\boldsymbol{\delta}_{\boldsymbol{\alpha}}(\zeta)$ incorporating the primary influence of the CCF, can be bounded in norm as

$$\left\|\boldsymbol{\delta}_{\boldsymbol{\alpha}}(\zeta)\right\|^2 \le \left(r^2_{\Delta\mathbf{P}}(\hat{\mathbf{t}}) \sum_{k=1}^{K} \left\|\nabla\alpha_k^{\mathscr{F}}(\boldsymbol{\tau})\right\|^2\right) \left\|\boldsymbol{\varphi}'(\zeta)\right\|^2, \tag{23}$$

where $\nabla\alpha_k^{\mathscr{F}}(\boldsymbol{\tau})$ is the gradient of the k^{th} component of the CCF, and $r_{\Delta\mathbf{P}}(\hat{\mathbf{t}})$ is a term that depends on the primary variation $\Delta\mathbf{P}$. In exercising a choice among available options for the CCF, it is desirable to minimize the CCF-dependent factor $(\sum_{k=1}^{K} \left\|\nabla\alpha_k^{\mathscr{F}}(\boldsymbol{\tau})\right\|^2)$ in the bound of (23) over the gamut. Based on this motivation, we consider two alternative, closely-related, optimization formulations for obtaining a CCF robust to primary variations.

A. Variational Formulation for Transition Preserving CCFs

An optimal transition preserving CCF $\boldsymbol{\alpha}^{\mathscr{F}}_{\Theta}(\cdot)$ can be formulated as the solution to the variational optimization

$$\begin{aligned} &\min\ \Theta(\boldsymbol{\alpha}^{\mathscr{F}}), \\ &\text{s.t. } \boldsymbol{\alpha}^{\mathscr{F}}(\boldsymbol{\tau}) \in \Omega(\mathbf{t}),\ \text{for all } \boldsymbol{\tau} \in \mathcal{G}_{\mathscr{F}}, \end{aligned} \tag{24}$$

where $\mathbf{t} = \mathscr{F}^{-1}_{\mathbf{w}}(\boldsymbol{\tau})$ and

$$\Theta(\boldsymbol{\alpha}^{\mathscr{F}}) = \int_{\mathcal{G}_{\mathscr{F}}} \sum_{k=1}^{K} \left\|\nabla\alpha_k^{\mathscr{F}}(\boldsymbol{\tau})\right\|^2 d\boldsymbol{\tau}. \tag{25}$$

is the CCF-dependent factor in the bound of (23). Note that the objective function penalizes CCFs with high-valued derivatives and therefore encourages smoothness of the CCF $\boldsymbol{\alpha}^{\mathscr{F}}_{\Theta}(\cdot)$ (as a function of coordinates $\boldsymbol{\tau}$ in the perceptual color space).

B. Variational Formulation for Transition Preserving CCF with Gray Axis Invariance

The accurate reproduction of colors along the gray axis ("neutral colors") is well-recognized as a key desirable attribute in color rendering. For instance, [36] states: "One of the most basic criteria for a good color reproduction process is that it be able to reproduce the neutral colors in a picture accurately." As already noted, *the CCF $\boldsymbol{\alpha}^{\mathscr{F}}_{\mathcal{A}}(\cdot)$ constructed in Section V-B maintains this desirable attribute even in the face of variations in the primaries, but has the deficiency that the CCF $\boldsymbol{\alpha}^{\mathscr{F}}_{\mathcal{A}}(\cdot)$ only assures continuity and does not ensure continuity of (first and higher order) derivatives, which is desirable for maintaining smoothness of smooth transitions in color in the presence of primary variations. We therefore consider an alternative optimization formulation for the CCF that uses an objective function that is a modification of the CCF-dependent factor in the bound of* (23) *such that deviations from the CCF $\boldsymbol{\alpha}^{\mathscr{F}}_{\mathcal{A}}(\cdot)$ are penalized in the vicinity of the gray axis*. Specifically, we formulate the problem of determining an optimal transition preserving CCF with gray axis invariance $\boldsymbol{\alpha}^{\mathscr{F}}_{\Gamma}(\cdot)$ as the solution to the variational optimization

$$\begin{aligned} &\min\ \Gamma(\boldsymbol{\alpha}^{\mathscr{F}}), \\ &\text{s.t. } \boldsymbol{\alpha}^{\mathscr{F}}(\boldsymbol{\tau}) \in \Omega(\mathbf{t}),\ \text{for all } \boldsymbol{\tau} \in \mathcal{G}_{\mathscr{F}}, \end{aligned} \tag{26}$$

where the objective function

$$\Gamma(\boldsymbol{\alpha}^{\mathscr{F}}) = \int_{\mathcal{G}} \sum_{k=1}^{K} \left\|\nabla\alpha_k^{\mathscr{F}}(\boldsymbol{\tau})\right\|^2 + \gamma\, I(\boldsymbol{\tau},\sigma) \left\|\boldsymbol{\alpha}^{\mathscr{F}}(\boldsymbol{\tau}) - \boldsymbol{\alpha}^{\mathscr{F}}_{\mathcal{A}}(\boldsymbol{\tau})\right\|^2 d\boldsymbol{\tau}, \tag{27}$$

is a modification of the CCF-dependent factor in the bound of (23) to penalize the deviation $\left\|\boldsymbol{\alpha}^{\mathscr{F}}(\boldsymbol{\tau}) - \boldsymbol{\alpha}^{\mathscr{F}}_{\mathcal{A}}(\boldsymbol{\tau})\right\|^2$ from the CCF $\boldsymbol{\alpha}^{\mathscr{F}}_{\mathcal{A}}(\cdot)$, weighed according to the function $\gamma\, I(\boldsymbol{\tau},\sigma)$. The weighting function $I(\boldsymbol{\tau},\sigma)$ can be chosen as a suitable continuous and differentiable function that localizes the penalty in deviation from the CCF $\boldsymbol{\alpha}^{\mathscr{F}}_{\mathcal{A}}(\cdot)$ to an appropriate local vicinity of the gray axis. As an example, the weighting function can be defined as the Gaussian function

$$I(\boldsymbol{\tau},\sigma) = e^{-\frac{1}{2}(C\boldsymbol{\tau}/\sigma)^2}, \tag{28}$$

where the parameter σ, the "standard deviation" of the Gaussian, and determines the rate at which the weighting decays with increasing chroma $C_{\boldsymbol{\tau}}$. Note that $I(\boldsymbol{\tau}, \sigma)$ is normalized such that $I([\tau_L, 0, 0]^T, \sigma) = 1$, so that the (nonnegative) parameter γ determines the weighting of the penalty term along the gray axis relative to the CCF-dependent factor in the bound of (23). A higher value of σ localizes the emphasis on agreement with the CCF $\boldsymbol{\alpha}_{\mathcal{A}}^{\mathscr{F}}(\cdot)$ to a narrower vicinity of the gray axis. A sample plot of the weighting function $I(\boldsymbol{\tau}, \sigma)$ is shown in Fig. 8 for $\sigma = 5$.

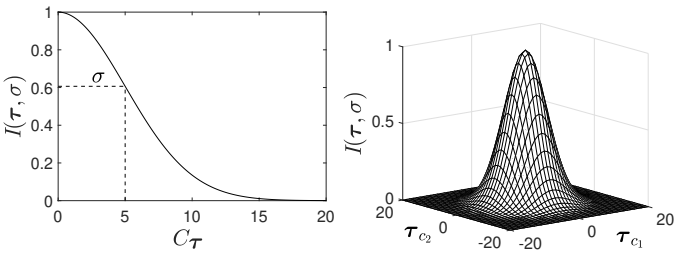

Fig. 8: Weighting function $I(\boldsymbol{\tau}, \sigma)$ of (27) illustrated for $\sigma = 5$.

Note that the objective function in (27) integrates two desirable features for a CCF $\boldsymbol{\alpha}^{\mathscr{F}}(\cdot)$ that boost robustness to primary variations: (1) smoothness, which was the basis of the objective function in (24) and (2) linearity along the gray axis, which was demonstrated to provide invariance to primary variations along the gray axis and used in the construction of the axially linear CCF in Section V.

VII. Conclusion

This paper introduced a framework for analyzing robustness of CCFs for multiprimary displays against primary and observer variations. Using the framework, we: (a) analytically demonstrated that linear CCFs offer invariance along the gray axis, and (b) constructed an axially linear CCF that is defined by the property of linearity along constant chromaticity loci and inherits the gray axis invariance. Within the proposed framework, we further analyzed the CCFs role in preserving rendered color transitions and demonstrated that smoothness of the CCF helps preserve color transitions in the renderings of continuous and differentiable color trajectories, despite primary/observer variations. Guided by the analysis, we proposed two alternative variational objective functions for optimizing CCFs for robustness against primary/observer variations. The first aims to preserve color transitions by encouraging smoothness of the CCF. The second combines this objective with desirable invariance along the gray axis, by incorporating the axially linear CCF. A companion Part II paper [20] presents an algorithmic approach for numerically computing optimal CCFs for the two alternative objective functions, illustrates sample optimal CCFs, and compares these to alternative CCFs for several different primary designs.

Appendix A
Attributes of Matrices Specifying the CCF $\boldsymbol{\alpha}_{\mathcal{A}}(\cdot)$

Applied to the $K = 3$ primary case, the pyramidal decomposition developed in Section V-C coincides with the obvious result $\boldsymbol{\alpha}_{\mathcal{A}}(\mathbf{t}) = \mathbf{P}^{-1}\mathbf{t}$ for all $\mathbf{t} \in \mathcal{G}$. This can be seen by noting that in the $K = 3$ primary setting, for any $\mathcal{A}$ quadrangle pyramid $\mathcal{Q}$, the parallelogram base of the pyramid has one of the primaries as the pyramid's origin $\mathbf{q}$ and the other two primaries constitute the vectors $\mathbf{p}_i$ and $\mathbf{p}_j$ that span the parallelogram base. The matrix $\mathbf{A}$ corresponds to a column permutation of the identity matrix. Using the fact that both $\mathbf{M}$ and $\mathbf{P}$ are nonsingular 3×3 matrices, (20) yields $\boldsymbol{\alpha}_{\mathcal{A}}(\mathbf{t}) = \mathbf{A}\left(\mathbf{PA}\right)^{-1}\mathbf{t} = \mathbf{P}^{-1}\mathbf{t}$.

Recall that for the $K = 3$ primary case, the gamut is a parallelepiped with $\mathbf{0}$ as its origin, i.e., having $\mathbf{0}$ as one of its vertices. The preceding result illustrates that the same matrix specifies the CCF for each of the $\mathcal{A}$ quadrangle pyramids for a 3 primary parallelepiped. In fact, a converse of this result also holds. For any arbitrary number of K primaries, if the same matrix specifies the CCF $\boldsymbol{\alpha}_{\mathcal{A}}(\cdot)$ over two $\mathcal{A}$ quadrangle pyramids, the two pyramids are $\mathcal{A}$ quadrangle pyramids in the parallelepiped gamut for a subset of three primaries (chosen from the K primaries). To see this, consider a couple of $\mathcal{A}$ quadrangle pyramids $\mathcal{Q}_1$ and $\mathcal{Q}_2$ for the K primary gamut, whose base parallelograms are spanned by primary pairs $(\mathbf{p}_{i_1}, \mathbf{p}_{j_1})$ and $(\mathbf{p}_{i_2}, \mathbf{p}_{j_2})$ and origins are given by $\mathbf{q}_1$ and $\mathbf{q}_2$, respectively. We denote by $\mathbf{A}_1, \mathbf{M}_1$ and $\mathbf{A}_2, \mathbf{M}_2$, the respective pairs of matrices that specify $\boldsymbol{\alpha}_{\mathcal{A}}(\cdot)$ within these pyramids. If the same matrix specifies the CCF $\boldsymbol{\alpha}_{\mathcal{A}}(\cdot)$ in these $\mathcal{A}$ quadrangle pyramids, we have $\mathbf{A}_1\mathbf{M}_1^{-1} = \mathbf{A}_2\mathbf{M}_2^{-1}$ and it follows that $\mathbf{A}_1 = \mathbf{A}_2\mathbf{M}_2^{-1}\mathbf{M}_1$. Note that $\mathbf{A}_1$ and $\mathbf{A}_2$ are matrices whose rows are vectors with zero-valued entries, with the possible exception of an entry that equals 1. Thus each row of $\mathbf{A}_1$ is either zero or a row selected from $\mathbf{M}_2^{-1}\mathbf{M}_1$, which is a nonsingular matrix. Furthermore, $\mathbf{A}_2$ has rank 3 therefore all three rows from $\mathbf{M}_2^{-1}\mathbf{M}_1$ need to be included as rows of $\mathbf{A}_1$. Thus conversely, the rows of $\mathbf{M}_2^{-1}\mathbf{M}_1$ can be obtained by selecting three rows from $\mathbf{A}_1$ and (by virtue of the rank constraint) are permutations of the rows of the 3×3 identity matrix. Thus, there is a 3×3 permutation matrix Λ such that $\mathbf{M}_2^{-1}\mathbf{M}_1 = \Lambda\mathbf{I}$. Equivalently, $\mathbf{M}_2 = \mathbf{M}_1\Lambda^{-1}$, that is, the columns of $\mathbf{M}_2$ are permutations of the columns of $\mathbf{M}_1$. As a consequence, the $\mathcal{A}$ quadrangle pyramids $\mathcal{Q}_1$ and $\mathcal{Q}_2$ are either the same ($\Lambda = \mathbf{I}$, or it permutes the second and third columns of $\mathbf{M}_1$), or they both belong to a parallelepiped spanned by primaries $\mathbf{q}_1, \mathbf{p}_{i_1}, \mathbf{p}_{j_1}$ ($\mathbf{q}_1$ and $\mathbf{q}_2$ are necessary primaries in this case, as Λ permutes the first column of $\mathbf{M}_1$). It follows that if the quadrangle pyramids $\mathcal{Q}_1$ and $\mathcal{Q}_2$ are distinct, $\mathbf{q}_1 = \mathbf{p}_{k_1}$ for some $1 \leq k_1 \leq K, k_1 \neq i_1, k_1 \neq j_1$, and the quadrangle pyramids $\mathcal{Q}_1$ and $\mathcal{Q}_2$ are $\mathcal{A}$ quadrangle pyramids in the parallelepiped gamut for the three primaries $\mathbf{p}_{i_1}, \mathbf{p}_{j_1}, \mathbf{p}_{k_1}$.

The preceding arguments imply that all $\mathcal{A}$ quadrangle pyramids in a gamut for which the CCF $\boldsymbol{\alpha}_{\mathcal{A}}(\cdot)$ is specified by the same matrix are $\mathcal{A}$ quadrangle pyramids in the parallelepiped gamut for a subset of three primaries. Therefore, the same matrix can specify the CCF $\boldsymbol{\alpha}_{\mathcal{A}}(\cdot)$ for at most three distinct $\mathcal{A}$ quadrangle pyramids, and by the convexity of the gamut, this limiting case is only possible for three primary displays. We note that for $K \geq 4$, there exist at least two $\mathcal{A}$ quadrangle pyramids for which the CCF $\boldsymbol{\alpha}_{\mathcal{A}}(\cdot)$ is specified by distinct matrices, and a single linear transform cannot specify the CCF

$\boldsymbol{\alpha}_{\mathcal{A}}(\cdot)$ over the entire gamut. Furthermore, because $\boldsymbol{\alpha}_{\mathcal{A}}(\cdot)$ is the unique CCF that is linear over constant chromaticity loci in the gamut, for $K \geq 4$ there is in fact no CCF that is a (single) linear transform over the entire gamut. A consequence of this statement is that for $K \geq 4$, every CCF will have a nonzero projection onto the CBS in some regions of the gamut.

As noted in Section V-C, over each quadrangle pyramid $\mathcal{Q}$, the CCF $\boldsymbol{\alpha}_{\mathcal{A}}(\cdot)$ is a linear function specified by the matrix $\mathbf{A}\mathbf{M}^{-1}$. As immediate consequences of this observation, within the quadrangle pyramid $\mathcal{Q}$, the CCF $\boldsymbol{\alpha}_{\mathcal{A}}(\cdot)$ is continuous and differentiable (to any order), with the Jacobian matrix (i.e., the matrix of first order partial derivatives) equal to $\mathbf{A}\mathbf{M}^{-1}$ and all second and higher order derivatives equal to 0. Note, however, that the linearity of the CCF $\boldsymbol{\alpha}_{\mathcal{A}}(\cdot)$ over adjacent quadrangle pyramids $\mathcal{Q}_1$ and $\mathcal{Q}_2$ does not assure continuity and differentiability over the boundary $\mathcal{Q}_1 \bigcap \mathcal{Q}_2$ between the adjacent pyramids. Continuity of the CCF $\boldsymbol{\alpha}_{\mathcal{A}}(\cdot)$ over the boundary $\mathcal{Q}_1 \bigcap \mathcal{Q}_2$ between adjacent quadrangle pyramids $\mathcal{Q}_1$ and $\mathcal{Q}_2$ can readily be seen by using the uniqueness of the CCF on the gamut surface in combination with the axially linear property of $\boldsymbol{\alpha}_{\mathcal{A}}(\cdot)$. However, we see that the Jacobian matrices for the CCF $\boldsymbol{\alpha}_{\mathcal{A}}(\cdot)$ over the pyramids $\mathcal{Q}_1$ and $\mathcal{Q}_2$ are, respectively, $\mathbf{A}_1\mathbf{M}_1^{-1}$ and $\mathbf{A}_2\mathbf{M}_2^{-1}$. This implies that the first order directional derivatives of the CCF $\boldsymbol{\alpha}_{\mathcal{A}}(\cdot)$ are discontinuous over the boundary $\mathcal{Q}_1 \bigcap \mathcal{Q}_2$ between adjacent quadrangle pyramids $\mathcal{Q}_1$ and $\mathcal{Q}_2$, unless the matrices $\mathbf{A}_1\mathbf{M}_1^{-1}$ and $\mathbf{A}_2\mathbf{M}_2^{-1}$ are identical. As already noted, for non-degenerate displays with $K \geq 4$ primaries, there exist quadrangle pyramids $\mathcal{Q}_1$ and $\mathcal{Q}_2$ for which the matrices $\mathbf{A}_1\mathbf{M}_1^{-1}$ and $\mathbf{A}_2\mathbf{M}_2^{-1}$ are distinct, and, therefore, there exist boundaries $\mathcal{Q}_1 \bigcap \mathcal{Q}_2$ between adjacent quadrangle pyramids $\mathcal{Q}_1$ and $\mathcal{Q}_2$ over which the CCF is not differentiable. Thus, in general, $\boldsymbol{\alpha}_{\mathcal{A}}(\cdot) \in C^0(\mathcal{G})$ but $\boldsymbol{\alpha}_{\mathcal{A}}(\cdot) \notin C^1(\mathcal{G})$. Note that the derivative discontinuities in $\boldsymbol{\alpha}_{\mathcal{A}}(\cdot)$ at boundaries between adjacent quadrangle pyramids manifest themselves in a directionally dependent fashion. At a point $\mathbf{t}_0 \in \mathcal{Q}_1 \bigcap \mathcal{Q}_2$, the directional derivative [37, pp. 136] along a (feasible) direction defined by a unit vector $\mathbf{v}$ has a discontinuity of magnitude $|\Delta\mathbf{J}\mathbf{v}|$, where $\Delta\mathbf{J} = \left(\mathbf{A}_1\mathbf{M}_1^{-1} - \mathbf{A}_2\mathbf{M}_2^{-1}\right)$. Note specifically, that the discontinuity is zero (or disappears) when $\mathbf{v}$ is in the null space of $\Delta\mathbf{J}$, which is the case when $\mathbf{t}_0 + \mathbf{v}$ is contained in $\mathcal{Q}_1 \bigcap \mathcal{Q}_2$, i.e., along trajectories lying in $\mathcal{Q}_1 \bigcap \mathcal{Q}_2$. The maximum magnitude discontinuity occurs when $\mathbf{v}$ matches the direction of the eigenvector with maximum eigenvalue for the matrix $\left(\Delta\mathbf{J}^T\Delta\mathbf{J}\right)$ [38].

Appendix B
Decomposition of the Deviation $\boldsymbol{\delta}(\cdot)$

This appendix develops a useful decomposition for the deviation function $\boldsymbol{\delta}(\zeta) = \hat{\boldsymbol{\varphi}}'(\zeta) - \boldsymbol{\varphi}'(\zeta)$. Using (21) and the definition of $\boldsymbol{\alpha}^{\mathscr{F}}(\cdot)$, we first write $\hat{\boldsymbol{\varphi}}(\zeta) = \mathscr{F}_{\mathbf{w}}\left(\mathbf{P}\boldsymbol{\alpha}\left(\mathscr{F}_{\bar{\mathbf{w}}}^{-1}\left(\boldsymbol{\varphi}(\zeta)\right)\right)\right)$ and via the chain rule, obtain

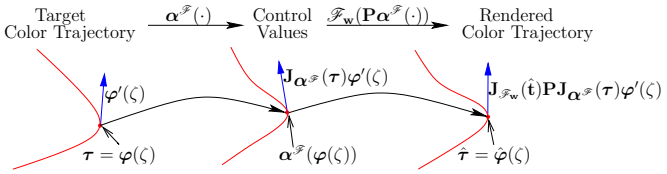

Fig. 9: Target $\boldsymbol{\varphi}(\cdot)$ and rendered $\hat{\boldsymbol{\varphi}}(\cdot)$ curves with their respective derivatives, at the different stages of color reproduction shown in Fig. 3. The derivative of the target curve at $\boldsymbol{\tau} = \boldsymbol{\varphi}(\zeta)$, for some $\zeta \in \mathbb{R}$, is the vector $\boldsymbol{\varphi}'(\zeta)$. The CCF $\boldsymbol{\alpha}^{\mathscr{F}}(\cdot)$ provides the control values for requested colors in the trajectory. These control values, in turn, are part of a curve in the control space whose derivative at $\boldsymbol{\alpha}^{\mathscr{F}}(\boldsymbol{\tau})$ is $\mathbf{J}_{\boldsymbol{\alpha}^{\mathscr{F}}}(\boldsymbol{\tau})\boldsymbol{\varphi}'(\zeta)$. When the display, with potential variation in the primaries, is driven by the control vector $\boldsymbol{\alpha}^{\mathscr{F}}(\boldsymbol{\tau})$ intended to reproduce $\boldsymbol{\tau}$, produces a color whose perceptual representation is $\hat{\boldsymbol{\tau}} = \hat{\boldsymbol{\varphi}}(\zeta)$, where $\hat{\boldsymbol{\varphi}}(\zeta) = \mathscr{F}_{\mathbf{w}}(\mathbf{P}\boldsymbol{\alpha}^{\mathscr{F}}(\boldsymbol{\varphi}(\zeta)))$ is the rendering of requested color trajectory, whose derivative can be expressed as $\hat{\boldsymbol{\varphi}}'(\zeta) = \mathbf{J}_{\mathscr{F}_{\mathbf{w}}}(\hat{\mathbf{t}})\mathbf{P}\mathbf{J}_{\boldsymbol{\alpha}^{\mathscr{F}}}(\boldsymbol{\tau})\boldsymbol{\varphi}'(\zeta)$.

$$\begin{aligned}
\hat{\boldsymbol{\varphi}}'(\zeta) =& \mathbf{J}_{\mathscr{F}_{\mathbf{w}}}(\hat{\mathbf{t}})\mathbf{P}\mathbf{J}_{\boldsymbol{\alpha}}(\mathbf{t})\mathbf{J}_{\mathscr{F}_{\bar{\mathbf{w}}}^{-1}}(\boldsymbol{\tau})\boldsymbol{\varphi}'(\zeta), && (29)\\
=& \mathbf{J}_{\mathscr{F}_{\mathbf{w}}}(\hat{\mathbf{t}})\bar{\mathbf{P}}\mathbf{J}_{\boldsymbol{\alpha}}(\mathbf{t})\mathbf{J}_{\mathscr{F}_{\bar{\mathbf{w}}}^{-1}}(\boldsymbol{\tau})\boldsymbol{\varphi}'(\zeta) + \\
& \mathbf{J}_{\mathscr{F}_{\mathbf{w}}}(\hat{\mathbf{t}})\Delta\mathbf{P}\mathbf{J}_{\boldsymbol{\alpha}}(\mathbf{t})\mathbf{J}_{\mathscr{F}_{\bar{\mathbf{w}}}^{-1}}(\boldsymbol{\tau})\boldsymbol{\varphi}'(\zeta). && (30)\\
=& \mathbf{J}_{\mathscr{F}_{\mathbf{w}}}(\hat{\mathbf{t}})\mathbf{J}_{\mathscr{F}_{\bar{\mathbf{w}}}^{-1}}(\boldsymbol{\tau})\boldsymbol{\varphi}'(\zeta) + \mathbf{J}_{\mathscr{F}_{\mathbf{w}}(\hat{\mathbf{t}})}\Delta\mathbf{P}\mathbf{J}_{\boldsymbol{\alpha}^{\mathscr{F}}}(\boldsymbol{\tau})\boldsymbol{\varphi}'(\zeta). && (31)
\end{aligned}$$

where $\mathbf{J}_{\mathbf{g}}(\mathbf{v})$ denotes the Jacobian of the function $\mathbf{g}(\cdot)$ at $\mathbf{v}$, $\mathbf{I}$ denotes the identity matrix, $\boldsymbol{\tau} = \boldsymbol{\varphi}(\zeta)$, $\mathbf{t} = \mathscr{F}_{\bar{\mathbf{w}}}^{-1}(\boldsymbol{\tau})$, $\hat{\mathbf{t}} = \mathbf{P}\boldsymbol{\alpha}(\mathbf{t})$, and in the final step we have used the fact that $\bar{\mathbf{P}}\mathbf{J}_{\boldsymbol{\alpha}}(\mathbf{t}) = \mathbf{I}$ and $\mathbf{J}_{\boldsymbol{\alpha}^{\mathscr{F}}}(\boldsymbol{\tau}) = \mathbf{J}_{\boldsymbol{\alpha}}(\mathbf{t})\mathbf{J}_{\mathscr{F}_{\bar{\mathbf{w}}}^{-1}}(\boldsymbol{\tau})$. Fig. 9 illustrates the concatenation of the different terms involved in (29) at different stages of the reproduction process.

Using (31), we obtain $\boldsymbol{\delta}(\zeta) = \boldsymbol{\delta}_0(\zeta) + \boldsymbol{\delta}_{\boldsymbol{\alpha}}(\zeta)$, with

$$\begin{aligned}
\boldsymbol{\delta}_0(\zeta) &= \left(\mathbf{J}_{\mathscr{F}_{\mathbf{w}}}(\hat{\mathbf{t}})\mathbf{J}_{\mathscr{F}_{\bar{\mathbf{w}}}^{-1}}(\boldsymbol{\tau}) - \mathbf{I}\right)\boldsymbol{\varphi}'(\zeta),\\
\boldsymbol{\delta}_{\boldsymbol{\alpha}}(\zeta) &= \mathbf{J}_{\mathscr{F}_{\mathbf{w}}(\hat{\mathbf{t}})}\Delta\mathbf{P}\mathbf{J}_{\boldsymbol{\alpha}^{\mathscr{F}}}(\boldsymbol{\tau})\boldsymbol{\varphi}'(\zeta). && (32)
\end{aligned}$$

From these expressions, we see that the primary influence of the CCF $\boldsymbol{\alpha}^{\mathscr{F}}(\cdot)$ is encapsulated in the second term $\boldsymbol{\delta}_{\boldsymbol{\alpha}}(\zeta)$, whereas the first term $\boldsymbol{\delta}_0(\zeta)$ depends on the CCF only indirectly through the changes in adaptation. Additionally, also note that $\mathbf{J}_{\mathscr{F}_{\bar{\mathbf{w}}}}(\mathbf{t})\mathbf{J}_{\mathscr{F}_{\bar{\mathbf{w}}}^{-1}}(\boldsymbol{\tau}) = \mathbf{I}$ and, therefore, for small primary variations the first term $\boldsymbol{\delta}_0(\zeta)$ tends to vanish independent of the CCF. The squared norm of the (second) term $\boldsymbol{\delta}_{\boldsymbol{\alpha}}(\zeta)$ can be bounded as

$$\begin{aligned}
\|\boldsymbol{\delta}_{\boldsymbol{\alpha}}(\zeta)\|^2 &\leq r_{\Delta\mathbf{P}}^2\left(\hat{\mathbf{t}}\right)\|\mathbf{J}_{\boldsymbol{\alpha}^{\mathscr{F}}}(\boldsymbol{\tau})\boldsymbol{\varphi}'(\zeta)\|^2,\\
&\leq r_{\Delta\mathbf{P}}^2\left(\hat{\mathbf{t}}\right)\|\boldsymbol{\varphi}'(\zeta)\|^2\sum_{k=1}^{K}\left\|\nabla\alpha_k^{\mathscr{F}}(\boldsymbol{\tau})\right\|^2, && (33)
\end{aligned}$$

where

$$r_{\Delta\mathbf{P}}^2\left(\hat{\mathbf{t}}\right) = \max_{\mathbf{v}\in\mathbb{R}^K,\ \|\mathbf{v}\|=1}\left\|\mathbf{J}_{\mathscr{F}_{\mathbf{w}}}\left(\hat{\mathbf{t}}\right)\Delta\mathbf{P}\mathbf{v}\right\|^2, \qquad (34)$$

is the ℓ^2 norm [39] of the matrix $\mathbf{J}_{\mathscr{F}_{\mathbf{w}}}\left(\hat{\mathbf{t}}\right)\Delta\mathbf{P}$, and the final step in obtaining (33), relied on the Cauchy inequality and

the observation that the vector $\mathbf{J}_{\boldsymbol{\alpha}^{\mathscr{F}}}(\boldsymbol{\tau})\boldsymbol{\varphi}'(\zeta)$ is the directional derivative of $\boldsymbol{\alpha}^{\mathscr{F}}(\boldsymbol{\tau})$ in the direction $\boldsymbol{\varphi}'(\zeta)$ [37, pp.147], whose k^{th} entry is $[\mathbf{J}_{\boldsymbol{\alpha}^{\mathscr{F}}}(\boldsymbol{\tau})\boldsymbol{\varphi}'(\zeta)]_k = \left(\nabla\alpha_k^{\mathscr{F}}(\boldsymbol{\tau})\right)^T \boldsymbol{\varphi}'(\zeta)$.

REFERENCES

[1] C. E. Rodríguez-Pardo and G. Sharma, "Multiprimary display color calibration: A variational framework for robustness to device variation," in *IS&T Electronic Imaging: Color Imaging XXI: Displaying, Processing, Hardcopy, and Applications*, vol. 2016, no. 20, San Francisco, California, Feb. 2016, pp. COLOR–304.1–7.

[2] T. Ajito, T. Obi, M. Yamaguchi, and N. Ohyama, "Expanded color gamut reproduced by six-primary projection display," in *Proc. SPIE: Projection Displays 2000: Sixth in a Series*, vol. 3954, San Jose, California, USA, Jan. 2000, pp. 13–0–137.

[3] H. Cheng, I. Ben-David, and S. Wu, "Five-Primary-Color LCDs," *Journal of Display Technology*, vol. 6, no. 1, pp. 3–7, 2010.

[4] M. Yamaguchi, T. Teraji, K. Ohsawa, T. Uchiyama, H. Motomura, Y. Murakami, and N. Ohyama, "Color image reproduction based on multispectral and multiprimary imaging: experimental evaluation," in *Proc. SPIE: Color Imaging: Device Independent Color, Color Hardcopy, and Applications VII*, vol. 4663, Jan. 2002, pp. 15–26.

[5] K. Yoshiyama, M. Teragawa, A. Yoshida, K. Tomizawa, K. Nakamura, Y. Yoshida, and Y. Yamamoto, "Power-saving: A new advantage of multi-primary color displays derived by numerical analysis," in *SID Symposium Digest of Technical Papers*, vol. 41, May 2010, pp. 416–418.

[6] C.-C. Tsai, F.-C. Lin, Y.-P. Huang, , and H.-P. D. Shieh, "RGBW 4-in-1 LEDs for backlight system for ultra-low power consumption field-sequential-color LCDs," in *SID Symposium Digest of Technical Papers*, vol. 41, May 2010, pp. 420–423.

[7] S. Ueki, K. Nakamura, Yuhichi, Yoshida, T. Mori, K. Tomizawa, Y. Narutaki, Y. Itoh, , and K. Okamoto, "Five-Primary-Color 60-inch LCD with novel wide color gamut and wide viewing angle," in *SID Symposium Digest of Technical Papers*, vol. 40, June 2009, pp. 927–930.

[8] M. Teragawa, A. Yoshida, K. Yoshiyama, S. Nakagawa, K. Tomizawa, and Y. Yoshida, "Review paper: Multi-primary-color displays: The latest technologies and their benefits," *J. Soc. Inf. Display*, vol. 20, no. 1, pp. 1–11, 2012.

[9] K. Tomizawa, K. Nakamura, S. Ueki, Y. Yoshida, T. Mori, M. Hasegawa, A. Yoshida, Y. Narutaki, Y. Itoh, Y. Yoshida *et al.*, "Multi-primary-color LCD: Its characteristics and extended applications," *J. Soc. Inf. Display*, vol. 19, no. 5, pp. 369–379, 2011.

[10] P. Centore and M. H. Brill, "Extensible multi-primary control sequences," *J. Soc. Inf. Display*, vol. 20, no. 1, pp. 12–21, 2012.

[11] T. Ajito, K. Ohsawa, T. Obi, M. Yamaguchi, and N. Ohyama, "Color conversion method for multiprimary display using matrix switching," *Opt. Rev.*, vol. 8, no. 2, pp. 191–197, 2001.

[12] D.-W. Kang, Y.-H. Cho, Y.-T. Kim, W.-H. Choe, and Y.-H. Ha, "Multiprimary decomposition method based on a three-dimensional look-up table in linearized LAB space for reproduction of smooth tonal change," *J. Imaging Sci. and Tech.*, vol. 50, no. 4, pp. 357–367, 2006.

[13] H. Motomura, "Color conversion for a multi-primary display using linear interpolation on equi-luminance plane method (LIQUID)," *J. Soc. Inf. Display*, vol. 11, no. 2, pp. 371–378, 2003.

[14] F. Konig, K. Ohsawa, M. Yamaguchia, N. Ohyama, and B. Hill, "A multiprimary display: Optimized control values for displaying tristimulus values," in *Proc. IS&T/SID PICS 2002: Image Processing, Image Quality, Image Capture Systems Conference*. Society for Imaging Science & Technology, 2002, pp. 215–220.

[15] H. Kanazawa, M. Mitsui, M. Yamaguchi, H. Haneishi, and N. Ohyama, "Color conversion for multi-primary displays using a spherical average method," in *Color and Imaging Conference*, vol. 2004, no. 1. Society for Imaging Science and Technology, 2004, pp. 65–69.

[16] M. Takaya, K. Ito, G. Ohashi, and Y. Shimodaira, "Color-conversion method for a multi-primary display to reduce power consumption and conversion time," *J. Soc. Inf. Display*, vol. 13, no. 8, pp. 685–690, 2012.

[17] P. Centore, "Minimal-energy control sequences for linear multi-primary displays," *J. Imaging Sci. and Tech.*, vol. 59, no. 5, pp. 50 502–1–10, 2015.

[18] C. E. Rodríguez-Pardo and G. Sharma, "Calibration sets for multiprimary displays: Representation, visualization, and applications," in *Proc. IS&T/SID 22nd Color and Imaging Conference*, Boston, MA, 3-7 Nov. 2014, pp. 171–179.

[19] T. Olson, "Smooth ramps: Walking the straight and narrow path through color space," in *Proc. IS&T/SID Seventh Color Imaging Conference: Color Science, Systems and Applications*, Scottsdale, AZ, 16-19 Nov. 1999, pp. 57–64.

[20] C. E. Rodríguez-Pardo and G. Sharma, "Color control functions for multiprimary displays II: Variational robustness optimization," *IEEE Trans. Image Proc.*, vol. 28, 2019, accepted for publication, to appear.

[21] G. Wyszecki and W. S. Stiles, *Color Science: Concepts and Methods, Quantitative Data and Formulae*, 2nd ed. New York: John Wiley & Sons, Inc., 1982.

[22] CIE, "Colorimetry," CIE Publication No. 15:2004, Central Bureau of the CIE, Vienna, 2004.

[23] H. J. Trussell, "DSP solutions run the gamut for color systems," *IEEE Sig. Proc. Mag.*, vol. 10, no. 2, pp. 8–23, Apr. 1993.

[24] G. Sharma and H. J. Trussell, "Digital color imaging," *IEEE Trans. Image Proc.*, vol. 6, no. 7, pp. 901–932, Jul. 1997.

[25] M. J. Vrhel and H. J. Trussell, "Color device calibration: A mathematical formulation," *IEEE Trans. Image Proc.*, vol. 8, no. 12, pp. 1796–1806, Dec. 1999.

[26] G. Sharma, "LCDs versus CRTs: Color-calibration and gamut considerations," *Proc. IEEE*, vol. 90, no. 4, pp. 605–622, Apr. 2002.

[27] S. R. Lay, *Convex sets and their applications*. Malabar, FL: Krieger Publishing Company, 1992.

[28] P. McMullen, "On zonotopes," *Trans. Amer. Math. Soc.*, vol. 159, pp. 91–109, 1971.

[29] H. Coxeter, *Regular polytopes*. New York, NY: Dover Publications, 1973.

[30] B. A. Wandell, *Foundations of Vision*. Sunderland, MA: Sinauer Associates, Inc., 1995.

[31] M. D. Fairchild, *Color Appearance Models*. Reading, MA: Addison-Wesley, 1998.

[32] N. Moroney, M. Fairchild, R. Hunt, C. Li, M. Luo, and T. Newman, "The CIECAM02 color appearance model," in *Proc. IS&T/SID Tenth Color Imaging Conference: Color Science, Systems and Applications*, Scottsdale, AZ, 12-15 Nov. 2002, pp. 23–27.

[33] C. Li, Z. Li, Z. Wang, Y. Xu, M. R. Luo, G. Cui, M. Melgosa, M. H. Brill, and M. Pointer, "Comprehensive color solutions: CAM16, CAT16, and CAM16-UCS," *Color Res. Appl.*, vol. 42, no. 6, pp. 703–718, 2017.

[34] S. Wen, "Design of relative primary luminances for four-primary displays," *Displays*, vol. 26, no. 4-5, pp. 171 – 176, 2005.

[35] P. Centore, "Non-metamerism of boundary colors in multi-primary displays," *J. Soc. Inf. Display*, vol. 20, no. 4, pp. 214–220, 2012.

[36] M. C. Stone, W. B. Cowan, and J. C. Beatty, "Color gamut mapping and the printing of digital color images," *ACM Trans. on Graphics*, vol. 7, no. 4, pp. 249–292, Oct. 1988.

[37] J. E. Marsden and A. Tromba, *Vector Calculus*, 6th ed. New York, NY: W.H. Freeman and Company, 2012.

[38] G. Strang, *Linear Algebra and its Applications*. New York, NY: Academic Press, 1976.

[39] G. H. Golub and C. F. V. Loan, *Matrix Computations*, 2nd ed. Baltimore, MD: The Johns Hopkins University Press, 1989.

Carlos Eduardo Rodríguez-Pardo received B.S. and M.S degrees in electronics engineering from Universidad de los Andes, Bogota, Colombia, and a M.S. degree in electrical and computer engineering from University of Rochester, Rochester, NY, where he is currently a PhD student. His research interests lie in the area of Color Imaging, the Human Visual System, and Image Processing.

Gaurav Sharma (S'88–M'96–SM'00–F'13) is at the University of Rochester with the Departments of Electrical and Computer Engineering, Computer Science and Biostatistics and Computational Biology. He is a fellow of the IEEE, of SPIE, and of the Society of Imaging Science and Technology (IS&T). Dr. Sharma serves as the Editor-in-Chief (EIC) for the IEEE Transactions on Image Processing (TIP) and previously served as the EIC for the Journal of Electronic Imaging (JEI) from 2011 through 2015.